



Western Washington University
Western CEDAR

WWU Honors Program Senior Projects

WWU Graduate and Undergraduate Scholarship

Spring 6-2018

Exploration of Peptide-Thiophene Hybrids as Self-Assembling Conductive Hydrogels

Ellie I. James
Western Washington University

Follow this and additional works at: https://cedar.wvu.edu/wwu_honors

 Part of the [Higher Education Commons](#)

Recommended Citation

James, Ellie I., "Exploration of Peptide-Thiophene Hybrids as Self-Assembling Conductive Hydrogels" (2018). *WWU Honors Program Senior Projects*. 92.
https://cedar.wvu.edu/wwu_honors/92

This Project is brought to you for free and open access by the WWU Graduate and Undergraduate Scholarship at Western CEDAR. It has been accepted for inclusion in WWU Honors Program Senior Projects by an authorized administrator of Western CEDAR. For more information, please contact westerncedar@wwu.edu.

Exploration of Peptide-Thiophene Hybrids as Self-Assembling Conductive Hydrogels

A Thesis
Presented to
The Faculty of
Western Washington University

In Partial Fulfillment
Of the Requirements for Honors Research for the Degree
Bachelor of Science

by
Ellie I. James
June 2018

Abstract

Abstract: Here, we have taken a bottom-up approach to confer multidimensional structure to conductive polymers by attaching thiophene monomers to peptides predicted to self-assemble into a biomimetic, fibrous nanostructure. A library of 12 peptides containing covalently attached thiophene-based monomers was synthesized. Peptide sequences that resulted in self-assembly and hydrogel formation in aqueous media were identified and the physical and electrical properties were characterized. The resulting hybrid materials have conductivities in the range of 10^{-2} - 10^{-3} S/cm, and possess moduli in the range of several tissue types, making them potential candidates for use in biomedical electronic applications.

Table of Contents

Abstract.....	i
List of Tables and Figures	iii
List of Abbreviations	v
Introduction.....	1
Materials and Methods.....	4
Results and Discussion.....	12
Conclusion	26
Works Cited.....	27
Appendix A	30
Appendix B	42
Appendix C.....	44

List of Tables and Figures

Figure 1	Chemical structures of peptide library	3
Table 1	Wang SPPS reactants	6
Table 2	Standard gel components	11
Figure 2	Illustration of gelation process.....	14
Table 3	Summary of gel quality.....	14
Figure 3	FTIR of lyophilized gelled peptides	16
Figure 4	Illustration of beta-sheet hydrogen bonding	16
Figure 5	SEM images of lyophilized unpolymerized gels	17
Figure 6	Photographs of gel polymerization progress.....	18
Figure 7	FTIR of lyophilized polymerized VDVA	19
Figure 8	SEM images of lyophilized polymerized gels	20
Table 4	Summary of polymerized gel electrical properties	21
Table 5	Summary of mechanical testing moduli	25
Figure 9	Plot of mechanical testing storage moduli outputs	25
Appendix A	Peptide Characterization	30-41
Figure 1 (AF1)	NMR spectrum of VEVA	30
Figure 2 (AF2)	NMR spectrum of VVEA	31
Figure 3 (AF3)	HPLC trace and NMR spectrum of VDVA	32
Figure 4 (AF4)	HPLC trace and NMR spectrum of VVDA	33
Figure 5 (AF5)	NMR spectrum of IEIA	34
Figure 6 (AF6)	HPLC trace and NMR spectrum of IIEA.....	35
Figure 7 (AF7)	HPLC trace and NMR spectrum of IDIA	36

Figure 8 (AF8)	HPLC trace and NMR spectrum of IIDA	37
Figure 9 (AF9)	NMR spectrum of FEFA.....	38
Figure 10 (AF10)	NMR spectrum of FFEA.....	39
Figure 11 (AF11)	NMR spectrum of LELA	40
Figure 12 (AF12)	NMR spectrum of LLEA	41
Appendix B	Phenylalanine and Leucine Gelation	42-44
Table 1 (BT1)	Phenylalanine and leucine gel study	43
Table 2 (BT2)	Buffered gel components	44
Figure 1 (BF1)	FTIR of wet FEFA gels.....	44
Appendix C	Additional Gel Characterization	45-46
Figure 1 (CF1)	FTIR of lyophilized polymerized gels	45
Equation 1	Sheet resistivity to resistivity	45
Equation 2	Resistivity to conductivity	45
Figure 2 (CF2)	Plot of mechanical testing loss moduli outputs.....	46
Figure 3 (CF3)	Plot of mechanical testing viscoelasticity outputs	46

List of Abbreviations

ATR	Attenuated total reflectance
CD	Circular dichroism spectroscopy
CP	Conductive polymer
DCM	Dichloromethane
DIPEA	<i>N, N'</i> -Diisopropylethylamine
DMF	<i>N, N'</i> -Dimethylformamide
EDOT-OH	(2,3-dihydrothieno[3,4- <i>b</i>][1,4]dioxin-2-yl)methanol
FEFA	Thiophene-phenylalanine-glutamic acid-phenylalanine-alanine
FFEA	Thiophene-phenylalanine-phenylalanine-glutamic acid-alanine
Fmoc	9-fluorenylmethoxycarbonyl
FTIR	Fourier transform infrared spectroscopy
HBTU	<i>N, N, N', N'</i> -tetramethyl-O-(1H-benzotriazol-1-yl)uranium hexafluorophosphate
IDIA	Thiophene-isoleucine-aspartic acid-isoleucine-alanine
IEIA	Thiophene-isoleucine-glutamic acid-isoleucine-alanine
IIDA	Thiophene-isoleucine-isoleucine-aspartic acid-alanine
IIEA	Thiophene-isoleucine-isoleucine-glutamic acid-alanine
HPLC	High performance liquid chromatography
LELA	Thiophene-leucine-glutamic acid-leucine-alanine
LLEA	Thiophene-leucine-leucine-glutamic acid-alanine
MS	Mass spectrometry
NMR	Nuclear magnetic resonance
PEDOT	Poly(3,4-ethylenedioxythiophene)
<i>p</i> -TSA	<i>para</i> -Toluene sulfonic acid
rt	Room temperature
SEM	Scanning electron microscopy
SPPS	Solid phase peptide synthesis
TFA	Trifluoroacetic acid
TIPS	Triisopropylsilane
VDVA	Thiophene-valine-aspartic acid-valine-alanine
VEVA	Thiophene-valine-glutamic acid-valine-alanine
VVDA	Thiophene-valine-valine-aspartic acid-alanine
VVEA	Thiophene-valine-valine-glutamic acid-alanine

Introduction

Biocompatible conducting polymers (CPs) and hybrid materials with integrated CPs are of great interest to the medical field due to their electrical properties and tissue compatibility. Metal electrodes coated with CPs have been shown to reduce the formation of scar tissue at the electrode/tissue interface, which allows coated electrodes to function longer and with less damage to the body than traditional electrodes.¹ However, the intrinsic brittleness associated with CPs due to their inflexible molecular structure gives rise to significant obstacles in the practicality of use beyond metal electrode coatings since CPs cannot be processed into useful 3D structures.² In response to this problem, the development of an easily processable biocompatible CP material would extend the practical use of CPs into bio-stimulation, neural recording, drug delivery and artificial tissues. By engineering a hybrid peptide-CP material with tunable properties and physical morphology, the use of CPs for fields such as neuroscience and prosthetics can be achieved.

Previous studies have shown that peptides with as few as four amino acid residues can assemble into fibrous gels in organic solvents that mimic the structure of soft tissues, giving rise to a hybrid material that could potentially be viable for *in vivo* applications.³ Other strategies have employed hydrogen-bonding interactions or pi-pi stacking of aromatic side chains to drive self-assembly into beta-sheets or beta-turns, which further associate into fibers.⁴⁻⁶ The combination of self-assembly motifs with CPs has led to the formation of hybrid materials featuring the desired electrical properties of the selected CP in a 3D network dictated by peptide self-assembly.⁷⁻⁹ Specifically, peptide-hybrids such as peptide-oligothiophene and peptide-3,4-ethylenedioxythiophene (EDOT) derivatives have been analyzed and shown to form canonical structures based upon the amino acid sequence of the peptide, though no electrical characterization has been previously reported.^{8,9} The Murphy group has extensively explored

hexyl-GAGA-EDOT and found that while it supports the beta-sheet self-assembly motif, it is a poor candidate for *in vivo* applications.¹⁰ Hexyl-GAGA-EDOT does not assemble in aqueous solution and has unsuitable mechanical properties for biomedical applications.

It would be advantageous to avoid organic solvents altogether, leading to the search for other peptide sequences that assemble in water and have robust physical and mechanical properties.¹¹⁻

¹³ Beta-sheet forming peptides often have the sequence (ZXZX)_n, where Z and X represent amino acid residues of alternating hydrophobicity.¹⁴ This alternation results in a peptide amphiphile with distinct faces; the hydrophobic faces tend to interact and sequester the hydrophobic side chains, presenting the hydrophilic residues on the opposite surface for interaction with solvent.¹⁴ The exposed hydrophilic face offers opportunity to initiate assembly with pH changes, increasing the likelihood of creating a peptide hydrogel. Sequences containing repeats of glycine (G) and alanine (A) form hydrogels with pH-dependent nanostructures, while those containing repeat units of valine (V) and threonine (T) have a strong tendency to form beta-sheets and aggregate into microscale fibrous structures.¹¹ Sequences containing glutamic acid (E) and V also exhibit strong beta-sheet character in aqueous media, making them promising candidates for gelation.¹¹

In our study, peptide sequences containing V and E were selected for their propensity to form beta-sheets in aqueous media.¹¹ Similarly, A was selected as the C-terminus amino acid in each peptide for its known presence in beta-sheet forming sequences and its apparent sensitivity to pH changes during gelation.¹¹ Isoleucine (I) and aspartic acid (D) offered variability in the length of the hydrophobic and acidic side chains by one carbon each. Leucine (L) offered additional variability in the length of the hydrophobic side chain, and phenylalanine (F) offered a rigid, hydrophobic structure capable of pi-stacking interactions. A library of 12 peptides was constructed from these amino acids based on three variables: identity of the hydrophobic residue,

identity of the acidic residue, and grouping of the hydrophobic residues (Figure 1). The identity of hydrophobic and acidic residues was systematically varied to test assembly strength based on side chain length, while hydrophobic residues were alternated to increase the size of the library and modulate the strength of assembly.

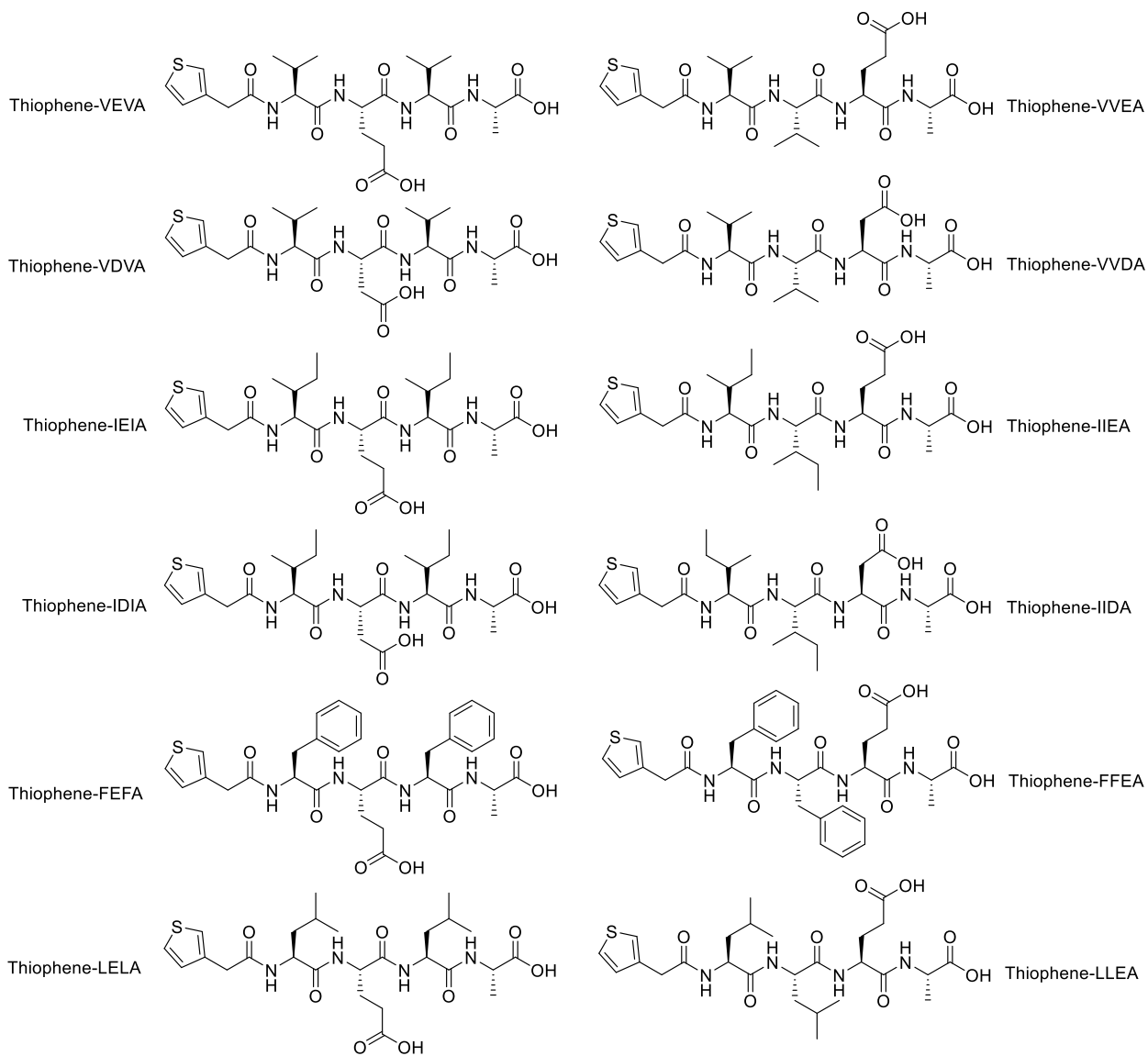


Figure 1. Chemical structures of the peptide library.

Here, we present the synthesis, characterization and evaluation of the 12-peptide library shown above. Eight of the 12 peptides were capable of gelation, and mechanical analysis indicates that this subset of peptides may also be injectable, increasing relevance for biomedical applications. Additionally, mechanical testing revealed gel densities compatible with human soft tissues, most notably brain and heart. All gels exhibiting self-assembly retained beta-sheet content and fibrous networks after polymerization and exhibited conductivity values on par with literature.

Materials and Methods

Chemicals and Instrumentation: All solvents and reagents were purchased from SigmaAldrich, EMDMillipore, AnaSpec, Strem Chemicals, Fisher Chemical, Novabiochem or Chem-Impex International and used without further purification. NMR data was collected on a Bruker 500 MHz spectrometer. FTIR spectra were collected using a Thermo Scientific Nicolet iS10 FRIT equipped with an attenuated total reflectance (ATR) accessory. HPLC-MS was performed on an Advion Expression LCMS with a Thermo Scientific Dionex UltiMate 3000 HPLC equipped with diode array UV-Vis spectrophotometer. Rheology experiments were performed with a TA Instruments Discovery Hybrid Rheometer-2 and TRIOS software. SEM imaging was performed on a Vega TS 5136MM SEM or JEOL JSM-7200F SEM. Resistivity measurements were made using a Lucas Labs Pro-4 four-point probe equipped with a Signatone SP4-40045TBY tip and powered by a Keithley 2400 SourceMeter.

Wang Solid Phase Peptide Synthesis (SPPS): The grams and moles of each reagent used are given in Table 1. Plastic fritted syringes (24 mL) were loaded with Wang-Ala-9-fluorenylmethoxycarbonyl (Fmoc) resin (0.71 mmol/g linker). The resin was rinsed twice with dichloromethane (DCM, 9 mL/rinse), and then rinsed 3x in *N,N*-dimethylformamide (DMF, 9 mL/rinse). To remove the Fmoc protecting group before each coupling, the resin-peptide was

soaked in 20% (v/v) piperidine/DMF (9 mL/rinse) for 5 min, rinsed with the same solution, then rinsed 3x with DMF. For each coupling, *N,N,N',N'*-tetramethyl-O-(1H-benzotriazol-1-yl)uronium hexafluorophosphate (HBTU) was combined with the appropriate amino acid or with 3-thiopheneacetic acid dissolved in 25% (v/v) diisopropylethylamine (DIPEA)/DMF (4.2 mL/coupling) for 5 min, then transferred to the fritted syringe to couple for 30 min. The finished peptide-thiophene derivatives were rinsed 3x with methanol, 3x with DMF, and 3x with DCM (9 mL/rinse). The peptides were then cleaved from the resin by soaking in 95% trifluoroacetic acid (TFA) containing 2.5% H₂O and 2.5% triisopropylsilane (TIPS) (9 mL) for 1 h. The peptide-TFA solution was eluted from the syringe, and the resin was rinsed twice more with the cleavage solution (9 mL/rinse). The TFA solution was removed by rotary evaporation, and each peptide was precipitated into -78 °C diethyl ether (100 mL), transferred to four 50 mL Falcon centrifuge tubes, and centrifuged for 10 min (4000 rpm at -4 °C). The supernatant was drained and discarded, and the pellets were resuspended twice in 20 mL cold ether, centrifuged, and drained. The pellets dried overnight or were dried under high vacuum (4 h), then were resuspended in nanopure H₂O (6 mL/tube) and lyophilized.

Table 1. Wang SPPS reactants

Reactant	Mass (g)	mmol
Wang-Ala-Fmoc Resin	0.500	0.355
HBTU	0.539	1.42
Fmoc-Val-OH	0.482	1.42
Fmoc-Ile-OH	0.502	1.42
Fmoc-Phe-OH	0.550	1.42
Fmoc-Leu-OH	0.502	1.42
Fmoc-Asp(OtBu)-OH	0.584	1.42
Fmoc-Glu(OtBu)-OH	0.604	1.42
3-thiopheneacetic acid	0.202	1.42

Thiophene-VEVA was isolated as a fluffy white solid (0.130 g, 68% yield); ATR-FTIR (lyophilized, neat): $\nu_{\max}/\text{cm}^{-1}$ 3278 (N-H), 2967 (sp^3 C-H), 1636 (amide I C=O), 1547 (amide II N-H bend), 1455 (C-H bend). $^1\text{H-NMR}$ (DMSO- d_6 , 500 MHz): δ (ppm) 0.80-0.92 (m, 9H), 1.26 (d, $J = 7.5$ Hz, 3H), 1.69-1.77 (m, 1H), 1.84-1.99 (m, 3H), 2.17-2.30 (m, 2H), 3.46-3.57 (m, 2H), 4.15-4.20 (m, 3H), 4.29-4.33 (m, 1H), 7.01-7.03 (m, 1H), 7.23-7.24 (m, 1H), 7.43-7.44 (m, 1H), 7.68 (d, $J = 10$ Hz, 1H), 8.05 (d, $J = 10$ Hz, 1H), 8.11 (d, $J = 10$ Hz, 1H) 8.22 (d, $J = 10$ Hz, 1H). ESI-MS m/z : 541.2 $[\text{M} + \text{H}]^+$ (calc. 541.2)

Thiophene-VVEA was isolated as a fluffy white solid (0.101 g, 52% yield); ATR-FTIR (lyophilized, neat): $\nu_{\max}/\text{cm}^{-1}$ 3273 (N-H), 2967 (sp^3 C-H), 1635 (amide I C=O), 1541 (amide II N-H bend), 1456 (C-H bend). $^1\text{H-NMR}$ (DMSO- d_6 , 500 MHz): δ (ppm) 0.80-0.87 (m, 12H), 1.26 (d, $J = 5$ Hz, 3H), 1.68-1.76 (m, 1H), 1.85-1.99 (m, 3H), 2.16-2.27 (m, 2H), 3.46-3.55 (m, 2H), 4.14-4.20 (m, 3H), 4.28-4.33 (m, 1H), 7.02 (d, $J = 5$ Hz, 1H), 7.23 (d, $J = 5$ Hz, 1H), 7.42-

7.44 (m, 1H), 7.85-7.91 (m, 1H), 8.05 (d, $J = 10$ Hz, 1H), 8.13 (d, $J = 10$ Hz, 1H). ESI-MS m/z : 541.2 $[M + H]^+$ (calc. 541.2)

Thiophene-VDVA was isolated as a white powder; ATR-FTIR (lyophilized, neat): $\nu_{\max}/\text{cm}^{-1}$ 3271 (N-H), 3079 (sp^2 C-H), 2962 (sp^3 C-H), 1704 (carboxylic acid C=O), 1633 (amide I C=O), 1539 (amide II N-H bend). $^1\text{H-NMR}$ (DMSO- d_6 , 500 MHz): δ (ppm) 0.79-0.99 (m, 12H), 1.26 (d, $J = 10$ Hz, 3H), 1.93-1.97 (m, 1H), 2.67-2.72 (m, 1H), 3.545-3.59 (m, 2H), 4.15-4.22 (m, 3H), 4.55-4.60 (m, 1H), 7.02 (dd, $J = 5, 5$ Hz, 1H), 7.24 (d, $J = 5$ Hz, 1H), 7.43-7.48 (m, 2H), 8.05 (d, $J = 5$ Hz, 1H), 8.21 (d, $J = 10$ Hz, 1H), 8.37 (d, $J = 10$ Hz, 1H), 12.38 (s, 2H). ESI-MS m/z : 527.2 $[M + H]^+$ (calc. 527.2)

Thiophene-VVDA was isolated as a white powder; ATR-FTIR (lyophilized, neat): $\nu_{\max}/\text{cm}^{-1}$ 3271 (N-H), 3079 (sp^2 C-H), 2962 (sp^3 C-H), 1704 (carboxylic acid C=O), 1634 (amide I C=O), 1539 (amide II N-H bend), 1453 (C-H bend). $^1\text{H-NMR}$ (DMSO- d_6 , 500 MHz): δ (ppm) 0.79-0.99 (m, 11H), 1.24 (d, $J = 5$ Hz, 3H), 1.92-1.98 (m, 2H), 2.65-2.69 (m, 1H), 3.46-3.56 (m, 2H), 4.13-4.22 (m, 3H), 4.54 (sextet, $J = 3$ Hz, 1H), 7.01 (m, 1H), 7.22-7.23 (m, 1H), 7.42-7.44 (m, 1H), 7.80 (d, $J = 5$ Hz, 1H), 7.91 (d, $J = 5$ Hz, 1H), 8.05 (d, $J = 5$ Hz, 1H), 8.17 (d, $J = 5$ Hz, 1H), 12.44 (s, 2H). ESI-MS m/z : 527.3 $[M + H]^+$ (calc. 527.2)

Thiophene-IEIA was isolated as a white powder (0.112 g, 53% yield); ATR-FTIR (lyophilized, neat): $\nu_{\max}/\text{cm}^{-1}$ 3279 (N-H), 3080 (sp^2 C-H), 2965 (sp^3 C-H), 1732 (carboxylic acid C=O), 1633 (amide I C=O), 1547 (amide II N-H bend), 1455 (C-H bend). $^1\text{H-NMR}$ (DMSO- d_6 , 500 MHz): δ (ppm) 0.76-0.86 (m, 12H), 1.08-1.11 (m, 2H), 1.26 (d, $J = 10$ Hz, 3H), 1.36-1.46 (m, 2H), 1.67-1.75 (m, 3H), 1.83-1.96 (m, 1H), 2.09-2.21 (m, 4H), 3.45-3.45 (m, 2H), 4.14-4.22 (m, 3H), 4.30 (sextet, $J = 5$ Hz, 1H), 7.01 (q, $J = 5$ Hz, 1H), 7.22-7.23 (m, 1H), 7.42-7.43 (m, 1H), 7.66 (d, $J =$

10 Hz, 1H), 8.07-8.12 (m, 2H), 8.24 (d, $J = 10$ Hz, 1H). ESI-MS m/z : 569.2 $[M + H]^+$ (calc. 569.3)

Thiophene-IIEA was isolated as a white powder; ATR-FTIR (lyophilized, neat): $\nu_{\max}/\text{cm}^{-1}$ 3270 (N-H), 3078 (sp^2 C-H), 2962 (sp^3 C-H), 1704 (carboxylic acid C=O), 1633 (amide I C=O), 1543 (amide II N-H bend), 1454 (C-H bend). $^1\text{H-NMR}$ (DMSO- d_6 , 500 MHz): δ (ppm) 0.76-0.99 (m, 11H), 1.08-1.11 (m, 2H), 1.26 (d, $J = 10$ Hz, 3H), 1.38-1.42 (m, 2H), 1.69-1.74 (m, 2H), 1.85-1.90 (m, 1H), 2.22-2.26 (m, 2H), 3.45-3.52 (m, 2H), 4.14-4.29 (m, 4H), 6.99 (q, $J = 5$ Hz, 1H), 7.21 (s, 1H), 7.42-7.44 (m, 1H), 7.89-7.92 (m, 1H), 8.08 (d, $J = 5$ Hz, 1H), 8.14 (d, $J = 5$ Hz, 1H), 12.31 (s, 2H). ESI-MS m/z : 569.3 $[M + H]^+$ (calc. 569.3)

Thiophene-IDIA was isolated as a white powder; ATR-FTIR (lyophilized, neat): $\nu_{\max}/\text{cm}^{-1}$ 3270 (N-H), 3078 (sp^2 C-H), 292 (sp^3 C-H), 1705 (carboxylic acid C=O), 1633 (amide I C=O), 1539 (amide II N-H bend), 1454 (C-H bend). $^1\text{H-NMR}$ (DMSO- d_6 , 500 MHz): δ (ppm) 0.76-0.84 (m, 12H), 0.94-1.09 (m, 3H), 1.27 (d, $J = 10$ Hz, 3H), 1.36-1.44 (m, 2H), 1.67-1.73 (m, 2H), 2.66-2.71 (m, 1H), 3.44-3.57 (m, 2H), 4.15-4.32 (m, 3H), 4.57-4.60 (m, 1H), 7.01 (d, $J = 5$ Hz, 1H), 7.23 (d, $J = 5$ Hz, 1H), 7.42-7.44 (m, 1H), 7.49 (d, $J = 10$ Hz, 1H), 8.07 (d, $J = 10$ Hz, 1H), 8.20 (d, $J = 5$ Hz, 1H), 8.37 (d, $J = 5$ Hz, 1H), 12.38 (s, 2H). ESI-MS m/z : 555.3 $[M + H]^+$ (calc. 555.2)

Thiophene-IIDA was isolated as a white powder in a previous synthesis; ATR-FTIR (lyophilized, neat): $\nu_{\max}/\text{cm}^{-1}$ 3270 (N-H), 3078 (sp^2 C-H), 2962 (sp^3 C-H), 1704 (carboxylic acid C=O), 1633 (amide I C=O), 1539 (amide II N-H bend), 1454 (C-H bend). $^1\text{H-NMR}$ (DMSO- d_6 , 500 MHz): δ (ppm) 0.76-0.80 (m, 12H), 1.03-1.07 (m, 3H), 1.25 (d, $J = 10$ Hz, 3H), 1.38-1.41 (m, 2H), 1.68-1.72 (m, 2H), 2.65-2.69 (m, 1H), 3.45-3.53 (m, 2H), 4.14-4.21 (m, 3H), 4.52-4.56

(m, 1H), 7.00 (d, $J = 5$ Hz, 1H), 7.22 (s, 1H), 7.42-7.44 (m, 1H), 7.82-7.89 (m, 2H), 8.08 (d, $J = 10$ Hz, 1H), 8.17 (d, $J = 10$ Hz, 1H). ESI-MS m/z : 555.3 $[M + H]^+$ (calc. 555.2)

Thiophene-LELA was isolated as a fluffy white solid (0.099 g, 49% yield); ATR-FTIR (lyophilized, neat): $\nu_{\max}/\text{cm}^{-1}$ 3274 (N-H), 3080 (sp^2 C-H), 2957 (sp^3 C-H), 1715 (carboxylic acid C=O), 1634 (amide I C=O), 1544 (amide II N-H bend), 1455 (C-H bend). $^1\text{H-NMR}$ (DMSO- d_6 , 500 MHz): δ (ppm) 0.78-0.88 (m, 12H), 1.26 (d, $J = 5$ Hz, 3H), 1.41-1.45 (m, 4H), 1.54-1.64 (m, 1H), 1.70-1.74 (m, 1H), 1.85-1.91 (m, 2H), 3.42-3.51 (m, 2H), 4.15-4.33 (m, 4H), 7.00 (d, $J = 5$ Hz, 1H), 7.22 (s, 1H), 7.42-7.43 (m, 1H), 7.79 (d, $J = 5$ Hz, 1H), 8.06 (d, $J = 5$ Hz, 1H), 8.15-8.19 (m, 2H).

Thiophene-LLEA was isolated as a fluffy white solid (0.098 g, 48% yield); ATR-FTIR (lyophilized, neat): $\nu_{\max}/\text{cm}^{-1}$ 3262 (N-H), 3079 (sp^2 C-H), 2958 (sp^3 C-H), 1714 (carboxylic acid C=O), 1630 (amide I C=O), 1540 (amide II N-H bend), 1452 (C-H bend). $^1\text{H-NMR}$ (DMSO- d_6 , 500 MHz): δ (ppm) 0.80-0.87 (m, 12H), 1.26 (d, $J = 5$ Hz, 3H), 1.42-1.46 (m, 4H), 1.53-1.59 (m, 2H), 1.74-1.75 (m, 1H), 1.87-1.91 (m, 1H), 2.23-2.26 (m, 2H), 3.42-3.49 (m, 2H), 4.15-4.18 (m, 1H), 4.24-4.32 (m, 3H), 6.99-7.00 (m, 1H), 7.21-7.22 (m, 1H), 7.42-7.44 (m, 1H), 7.79 (d, $J = 10$ Hz, 1H), 8.01 (d, $J = 10$ Hz, 1H), 8.14-8.19 (m, 2H).

Thiophene-FEFA was isolated as a fluffy white solid (0.154 g, 68% yield); ATR-FTIR (lyophilized, neat): $\nu_{\max}/\text{cm}^{-1}$ 3281 (N-H), 3064 (sp^2 C-H), 1711 (carboxylic acid C=O), 1633 (amide I C=O), 1520 (amide II N-H bend), 1454 (C-H bend). $^1\text{H-NMR}$ (DMSO- d_6 , 500 MHz): δ (ppm) 1.29 (d, $J = 10$ Hz, 3H), 1.65-1.73 (m, 1H), 1.80-1.87 (m, 1H), 2.12-2.20 (m, 2H), 2.68-2.81 (m, 2H), 2.95 (dd, $J = 12.5, 5$ Hz, 1H), 3.06 (dd, $J = 12.5, 5$ Hz, 1H), 3.38 (q, $J = 10$ Hz, 2H), 4.21 (quint, $J = 5$ Hz, 2H), 4.50-4.57 (m, 2H), 6.80 (dd, $J = 5, 5$ Hz, 1H), 7.02 (s, 1H), 7.14-

7.36 (m, 10H), 7.93 (d, $J = 10$ Hz, 1H), 8.10 (d, $J = 5$ Hz, 1H), 8.21 (d, $J = 10$ Hz, 1H), 8.32 (d, $J = 10$ Hz, 1H).

Thiophene-FFEA was isolated as a fluffy white solid (0.110 g, 49% yield); ATR-FTIR (lyophilized, neat): $\nu_{\max}/\text{cm}^{-1}$ 3285 (N-H), 2931 (sp^3 C-H), 1710 (carboxylic acid C=O), 1632 (amide I C=O), 1520 (amide II N-H bend), 1452 (C-H bend). $^1\text{H-NMR}$ (DMSO- d_6 , 500 MHz): δ (ppm) 1.26 (d, $J = 5$ Hz, 3H), 1.74-1.81 (m, 1H), 1.88-1.95 (m, 1H), 2.28 (t, $J = 10$ Hz, 2H), 2.68-2.72 (m, 1H), 2.79-2.84 (m, 1H), 2.95-3.04 (m, 2H), 3.38 (q, $J = 10$ Hz, 2H), 4.19 (sextet, $J = 5$ Hz, 1H), 4.30-4.42 (m, 1H), 4.48-4.58 (m, 2H), 6.77-6.79 (m, 1H), 6.99 (s, 1H), 7.14-7.29 (m, 10H), 7.35-7.36 (m, 1H), 8.07 (d, $J = 5$ Hz, 1H), 8.13 (d, $J = 5$ Hz, 1H), 8.18 (d, $J = 5$ Hz, 1H), 8.23 (d, $J = 10$ Hz, 1H).

Gelation Procedure: Table 2 lists the specific amounts of the reagents used for this procedure. Lyophilized peptide-thiophene derivatives and (2,3-dihydrothieno[3,4-b][1,4]dioxin-2-yl)methanol (EDOT-OH, 1:1 mol ratio) were weighed into 4.5 mL polypropylene shell vials. Nanopure H_2O and NaOH (1 M) were added until the peptide was fully solubilized upon sonication. *p*-TSA (0.2 M) was added to the solution while sonicating to induce gelation (Table 4). Gels formed immediately following acidification except in the case of VVEA, which was left to rest for 1 d at rt before gelation was assessed. Gels were stored tightly capped at rt and allowed to rest a minimum of 4 h before characterization.

Table 2. Standard components for 1% (w/v) gels

Peptide	Peptide Mass (mg)	EDOT-OH Mass (mg)	np H ₂ O (μL)	1 M NaOH (μL)	0.2 M <i>p</i> -TSA (μL)
VEVA	5.0	1.6	339	23.0	138
VVEA	5.0	1.6	339	23.0	138
IEIA	5.0	1.5	345	22.0	133
IIEA	5.0	1.5	345	22.0	133
VDVA	5.0	1.6	345	22.0	133
VVDA	5.0	1.6	345	22.0	133
IDIA	5.0	1.5	351	21.0	128
IIDA	5.0	1.5	351	21.0	128

Polymerization Procedure: Homogenous gels were injected at rt with a 40 μL FeCl₃ solution (1:1 mol ratio FeCl₃:CP) using a 27 gauge needle. The needle was used to pierce the body of the gel, and the solution was slowly and evenly injected as the needle was withdrawn from the gel. The gels were then capped and placed in a 50 °C incubator until polymerization was complete (48 h). Polymerized gels were rinsed gently 3x with 1 mL npH₂O, then soaked 3x in 1.5 mL npH₂O (20 min); washes were discarded and polymerized gels were stored at room temperature.

Rheological Testing Parameters: Mechanical testing was performed on 1% (w/v) gels at 37 °C. Enough gel was added to fill the 25-mm parallel plates at a gap distance of 530 μm, after which a fixed strain of 0.05 or 0.1% was applied from 0.1-10 Hz for 5 data points/decade as the result of 3 iterative trials/point with 5% tolerance. Storage and loss moduli were recorded alongside complex viscosity and averaged by gel identity. Data was collected in triplicate and averaged unless otherwise noted.

Conductivity Testing: Conductivity testing was performed on polymerized gels after washing gently with water to remove residual monomer and excess FeCl₃. Gels were lyophilized and pellet-pressed, then analyzed via 4-point probe. Ten resistance data points were collected and averaged, then converted to resistivity using the thickness of the pellet (Appendix C, Equations 1 and 2).

SEM Images: Gelled peptide derivatives were lyophilized and individually applied to carbon tape on SEM stubs. Polymerized gel samples were washed gently, lyophilized and individually applied to carbon tape on SEM stubs. The stubs were dried by vacuum desiccator overnight. Samples were sputter coated for 60 or 90 s with a Pd/Au mixture. Images were captured at magnifications ranging between 1 kx and 75 kx for each peptide. Imaging on the Vega TS 5136MM SEM was performed at an accelerating voltage of 15 kV. Imaging performed on the JEOL JSM-7200F SEM utilized either SEM mode with an accelerating voltage between 3 and 20 kV, or in gentle beam mode with an accelerating voltage of 1 kV.

Results and Discussion

Peptide Synthesis, Purification, and Characterization

The 12 tetrapeptide derivatives shown in Figure 1 were synthesized on Wang resin using standard Fmoc-based methods. Each peptide was N-acylated using 3-thiopheneacetic acid while on-resin. The peptides were precipitated and washed with ether, dried, lyophilized and used with no further purification. Peptide structure and purity were analyzed by NMR and HPLC-MS (Appendix A).

Gelation

As outlined in Figure 2, gels were created by combining the lyophilized peptide and EDOT-OH in water to make a 1% (w/v) peptide solution. A small aliquot of sodium hydroxide (NaOH, 1M) was added to solubilize the peptides. This mixture was sonicated until the peptide and EDOT-OH had fully dissolved, after which an aqueous solution of *para*-toluenesulfonic acid (*p*-TSA, 0.2 M) was added to induce gelation. *p*-TSA was used as the acid to protonate the peptide and serve as a dopant for the subsequent polymerization reactions. The resulting homogenous gels were subjected to characterization after resting a minimum of 4 h at room temperature. While the majority of the peptides containing V and I hydrophobic residues consistently formed homogeneous gels, VEVA and IEIA occasionally formed heterogeneous, segmented gels (Table 3). Successful gels had optical properties ranging from opaque to transparent. In general, gels containing a D moiety were more transparent than those containing an E moiety. The four D derivatives were either transparent in the case of VDVA and VVDA, or nearly transparent in the case of IDIA and IIDA. VEVA gels were opaque, and the IEIA and IIEA gels were nearly opaque (Table 3). Gelation of L and F peptides was attempted unsuccessfully. L-based peptides immediately precipitated out of solution with the addition of acid, while F-based gels formed transiently but collapsed over the course of several hours (Table 3, Appendix B). Due to their inability to stably self-assemble, exploration of the four peptides containing L or F was discontinued.

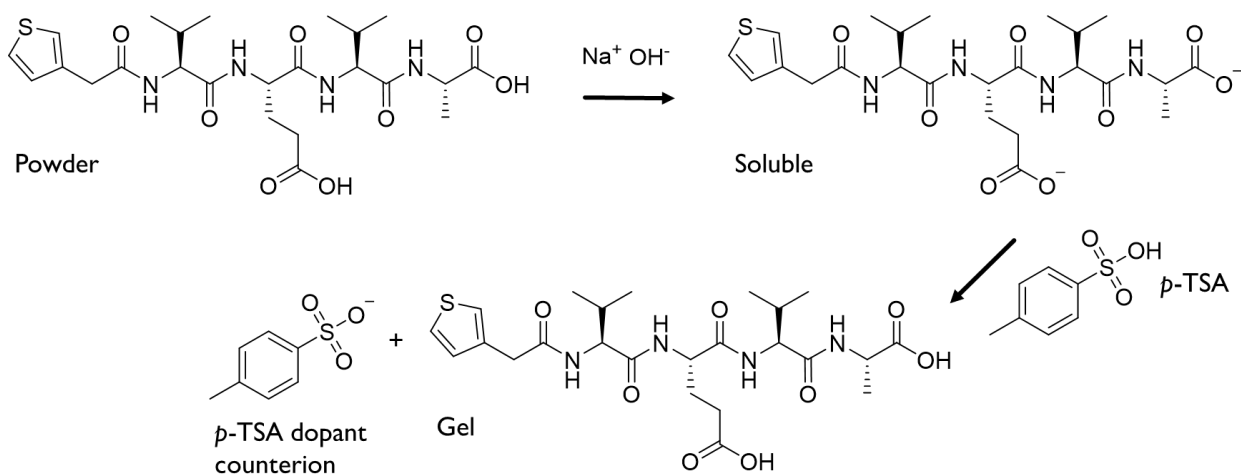


Figure 2. Representative gelation process illustrated with VEVA.

Table 3. Average quality of 1% (w/v) gels pre- and post-polymerization.

Peptide	Homogeneity	Clarity	Stability	Polymerized Stability
VEVA	Often	5	Strong	Variable
VVEA	Always	3	Moderate	Moderate
VDVA	Always	1	Strong	Strong
VVDA	Always	1	Strong	Strong
IEIA	Often	4	Strong	Strong
IIEA	Always	4	Weak	Variable
IDIA	Always	2	Strong	Strong
IIDA	Always	2	Weak	Strong
LELA	Precipitate	5	N/A	N/A
LLEA	Precipitate	5	N/A	N/A
FEFA	Transient	5	Weak	N/A
FFEA	Transient	5	Weak	N/A

1 = Transparent 3 = Translucent 5 = Opaque

Fourier transform infrared spectroscopy (FTIR) was performed on lyophilized gels to detect the presence of secondary structure. *p*-TSA peaks present from acidification were observed below 1450 cm^{-1} and contributed to sp^2 and sp^3 C-H stretching peaks. All gels exhibited N-H stretching modes near 3275 cm^{-1} , sp^2 C-H stretching near 3060 cm^{-1} , sp^3 C-H stretching between 2850 cm^{-1} and 3000 cm^{-1} , a carboxylic acid C=O stretch near 1715 cm^{-1} , an amide I (C=O) peak near 1630 cm^{-1} , and an amide II (N-H bend) peak near 1540 cm^{-1} (Figure 3). The amide I peak is diagnostic of secondary structure in proteins and peptides; an amide I peak between 1620 cm^{-1} and 1629 cm^{-1} with a weak shoulder near 1695 cm^{-1} indicates antiparallel beta-sheets, while an amide I peak between 1620 cm^{-1} and 1629 cm^{-1} with a weak shoulder near 1640 cm^{-1} indicates parallel beta-sheets (Figure 4).¹⁵ An amide I peak observed above 1650 cm^{-1} indicates the presence of alpha-helices or disorder. The amide I peak of the 8 peptides that formed gels fell between 1629 cm^{-1} and 1633 cm^{-1} , suggesting the presence of beta-sheets. However, no obvious shoulders were observed that would distinguish parallel from anti-parallel beta-sheets. Circular dichroism (CD) spectroscopy could be used to address the orientation of beta-sheets, however, the thiophene moiety covalently attached to the N-termini of the peptides has a UV absorbance that interferes with secondary structure determination by CD.

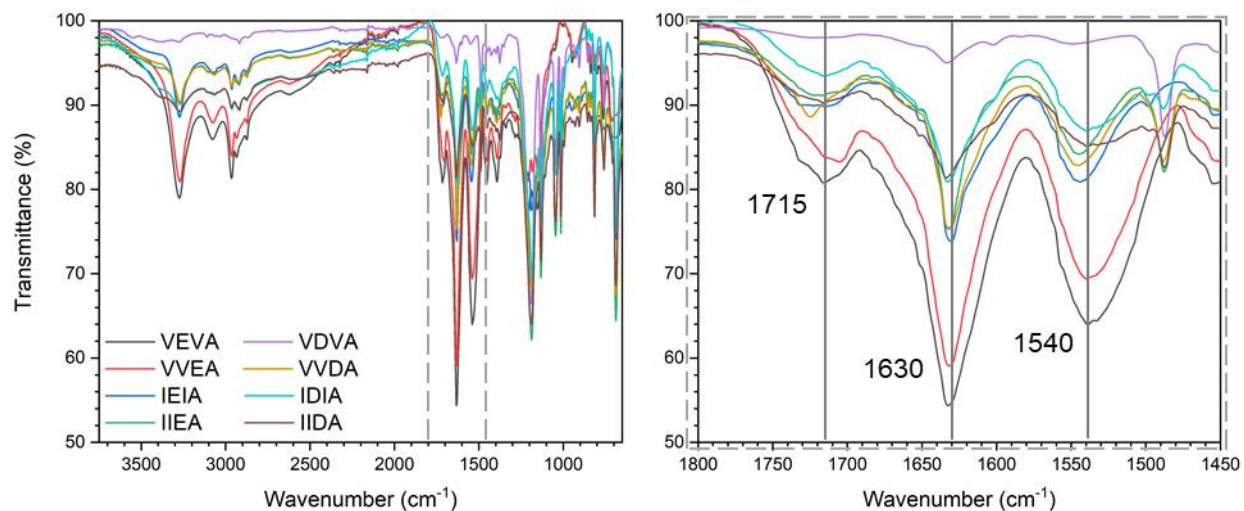


Figure 3. FTIR spectra of gelled peptides indicating assembly into beta-sheets.

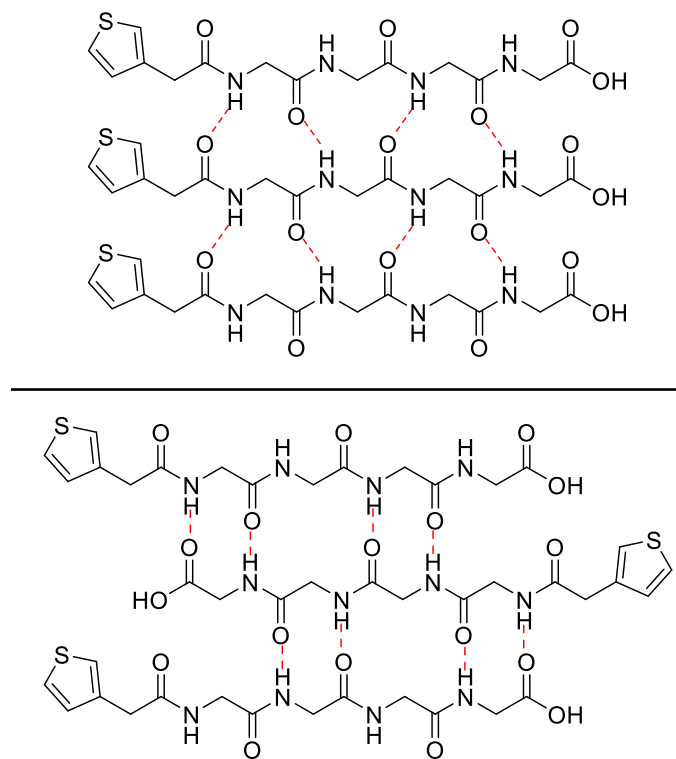


Figure 4. Arrangement of molecules in parallel (top) and antiparallel (bottom) beta-sheets.

SEM images were collected of lyophilized gels prior to polymerization to characterize physical properties and assess the presence of a fibrous, biomimetic structure. Several peptide gels remain to be characterized by SEM. Of those gels characterized, low magnification imaging reveals both sheet-like and globular morphologies. These features vary in size between gels, but variation appears determined by sample preparation and handling and does not seem to signify an intrinsic property of the gel. A representative low magnification image of unpolymerized VDVA (Figure 5A) reveals sheets and indicates some porosity. Higher magnification imaging of the same sample (Figure 5B) reveals the presence of fibers, suggesting that fibers compose the larger structures observed in low magnification imaging. These fibers form through the association of beta-sheets.

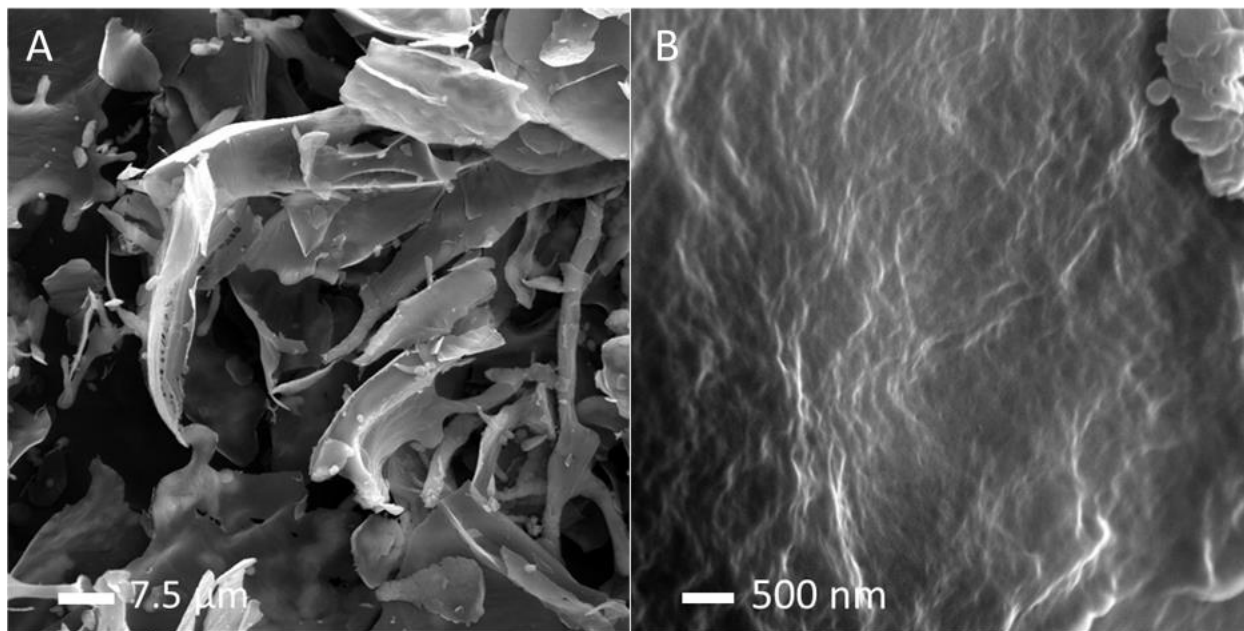


Figure 5. Representative SEM images of unpolymerized VDVA at A) low magnification revealing microscale morphology, and at B) high magnification revealing a nanoscale fibrous morphology.

Gel Polymerization and Electrical Characterization

To polymerize the gels and render them conductive, homogenous gels were injected with a solution of iron (III) chloride (FeCl_3), then incubated at 50 °C for 48 h (Figure 6). The polymerized gels were rinsed gently with water prior to characterization. Polymerization disrupted VEVA and IIEA gels in some cases, resulting in a collapse of the 3D structure or a loss of robustness accompanied by a change in texture from smooth to gritty (Table 3). This structural failure was observed most frequently in IIEA, which was the gel with the lowest storage modulus before polymerization and the second lowest after polymerization (Table 5). VEVA also exhibited periodic disruption during polymerization, contrary to the mid-level storage modulus observed both before and after polymerization associated with VEVA gels.

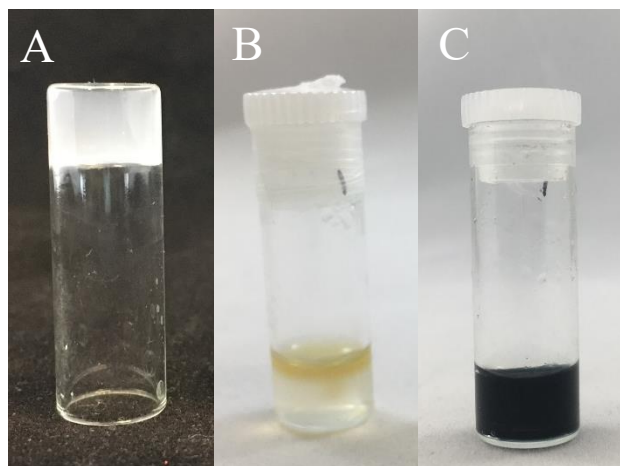


Figure 6. Representatives photographs of the gel polymerizations. VVDA gel **A)** before, **B)** during, and **C)** after polymerization.

FTIR spectroscopy was performed on lyophilized polymerized gels to analyze retention of secondary structure after polymerization. Spectra of VDVA before and after polymerization are shown in Figure 7, and are representative of all the gels (See Appendix C, F1 for the complete

set of spectra). *p*-TSA peaks were observed below 1450 cm⁻¹ and contributed to the sp² and sp³ C-H stretching peaks. All gels exhibited N-H stretching modes near 3275 cm⁻¹, weak sp² C-H stretching near 3060 cm⁻¹, sp³ C-H stretching between 2850 cm⁻¹ and 3000 cm⁻¹, a carbonyl C=O stretch near 1715 cm⁻¹, an amide I peak near 1630 cm⁻¹, and an amide II peak near 1540 cm⁻¹ (CF1, Figure 7). These positions of these peaks match well with the observed peaks in unpolymerized gel samples, indicating that the polymerization process did not impact gel assembly. Specifically, the amide I peaks did not shift away from 1630 cm⁻¹, confirming retention of beta-sheets after polymerization. Following polymerization, gels are insoluble and could not be analyzed through alternative spectroscopic methods.

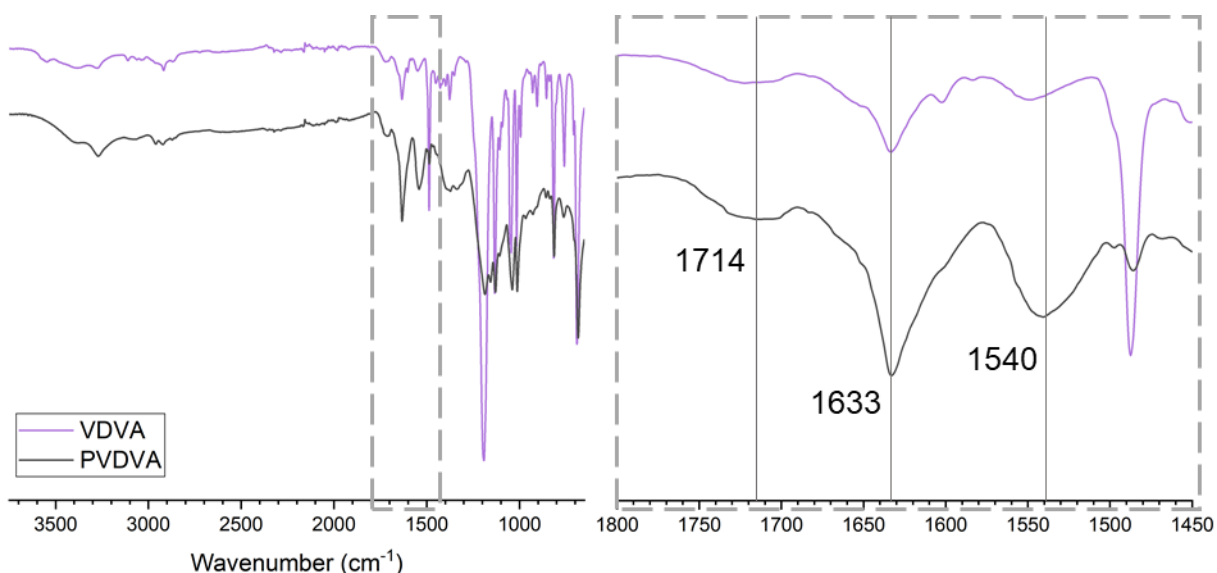


Figure 7. FTIR spectra of VDVA pre- and post-polymerization indicating retention of beta-sheet assembly. See also CF1.

SEM imaging of gels was performed to analyze gel morphology post-polymerization. Figure 8A shows unpolymerized VDVA (also shown in Figure 5B) next to polymerized VDVA (Figure

8B) at a similar magnification. Fibers are evident in PVDVA, supporting the conclusion that polymerization did not disrupt beta-sheet assembly. High magnification imaging of PVVDA (Figure 8D) shows an entangled fiber network with fiber diameters measured between 7 and 15 nm. This fibrous network would allow nutrient exchange if a polymerized gel were implanted into human tissue, validating the design criteria selected to encourage peptide beta-sheet assembly.

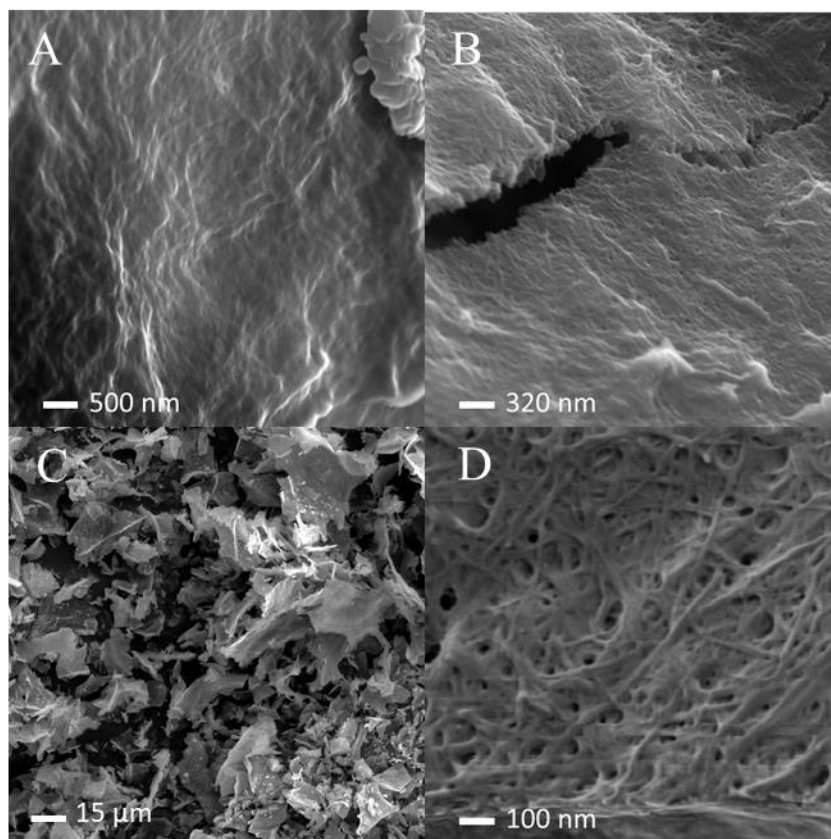


Figure 8. SEM micrographs of fibrous networks shown **A)** in VDVA before polymerization, **B)** in VDVA after polymerization, **C)** at low magnification in VVDA after polymerization, and **D)** at high magnification in PVVDA. PVVDA fibers ranged between 7 and 15 nm in diameter.

Conductivity Testing

Conductivity testing was performed on polymerized gels after washing gently with water to remove residual monomer and excess FeCl₃. Each gel was lyophilized then compressed into a pellet and analyzed by 4-point probe to determine sheet resistivity. Sheet resistivity was converted into resistivity, then to conductivity according to Equation 1 and 2 (Appendix C). All library members displayed conductivity of approximately 10⁻² S/cm (Table 4), reaching the low end of the PEDOT range (10⁻² – 10² S/cm) and approaching that of undoped silicon (10⁻¹ S/cm). These values are comparable to or better than literature hydrogel conductivity values using thiophene-based CPs with polymer-based hydrogels and comparable to values obtained using polydopamine-carbon-nanotube hydrogels.¹⁶⁻¹⁸ Each of the eight library members have conductivity at least one order of magnitude greater than recently published papers concerning peptide-CP hydrogels.¹⁰ There does not appear to be a correlation between conductivity and assembly strength (Tables 4, 5).

Table 4. Electrical properties of gels

	VEVA	VVEA*	IEIA*	IIEA*	VDVA	VVDA	IDIA	IIDA*
ρ ($\Omega\cdot\text{cm}$)	367	102	450	119	118	110	66.5	105
σ (S/cm)	3.1E-3	9.9E-3	2.2E-3	8.4E-3	8.5E-3	9.1E-3	1.5E-2	9.6E-3

* One trial

Unmarked: Two trials

Rheological Testing

Mechanical testing was performed on 1% gels of each peptide before and after polymerization. Eight gels were produced from each peptide, half of which were subsequently polymerized following standard procedure. Rheology was then performed using parameters developed from literature standards and adapted to the moduli of the peptide hydrogels.^{18,19} Briefly, gels were oscillated at varying frequency with a fixed strain percent within the viscoelastic region of each gel. Reported values are the average of triplicate trials irrespective of the frequency at which the point was collected.

Mechanical testing results (Table 5, Figure 9, Appendix C: CF2, CF3) did not offer a clear pattern for determining the storage modulus of a gel from its peptide sequence, though several intermediate conclusions have been reached. First, I-based gels with grouped hydrophobic residues (IIEA, IIDA) possessed the lowest overall storage moduli at 20.0 ± 5.7 kPa and 35.5 ± 9.0 kPa respectively before polymerization, nearly an order of magnitude lower than the isomeric peptides with alternating hydrophobicity (IDIA, IEIA) which had resultant storage moduli of 97.8 ± 14.5 kPa and 94.7 ± 7.8 kPa before polymerization. Polymerization resulted in storage moduli of 44.0 ± 14.2 kPa (PIEIA) and 80.6 ± 19.0 kPa (PIDIA) for the I-based gels with alternating hydrophobicity, while the I-based gels with grouped hydrophobic residues retained the lowest storage moduli after polymerization at measured values of 28.0 ± 8.7 kPa and 27.8 ± 5.3 kPa (PIIDA). These results indicate that I-based gels assemble more robustly when the hydrophobic residues alternate with the hydrophilic residues.

A conclusive pattern was not observed in the behavior of I-based peptide assembly with consideration to the acidic residue present in the peptide. With measured storage moduli of 97.8 ± 14.5 kPa (IEIA) versus 94.7 ± 7.8 kPa (IDIA) and 20.0 ± 5.7 kPa (IIEA) versus 35.5 ± 9.0 kPa (IIDA) before polymerization, the storage moduli range of peptides with the same

hydrophobicity pattern and different acidic residue identity overlap or nearly overlap. Polymerized gels exhibited storage moduli of 44.0 ± 14.2 kPa (PIEIA) versus 80.6 ± 19.0 kPa (PIDIA) and 28.0 ± 8.7 kPa (PIIEA) versus 27.8 ± 5.3 kPa (PIIDA), indicating a potential preference for D in the I-based gels with alternating hydrophobic groups (PIEIA, PIDIA). However, the large error margins associated with PIEIA and PIDIA suggest that more testing is necessary before concluding the difference in I-based gel strength related to the acidic residues is significant. Additionally, the 50.7 kPa decrease in modulus observed after polymerization in IEIA gels (94.7 kPa to 44.0 kPa) may indicate that data for the PIEIA samples is not representative of the true assembly strength of those gels. A larger sample size is necessary before determining a pattern based on the identity of the acidic residue in I-based gels.

Contrary trends were observed in the storage moduli of V-based gels compared to those of I-based gels. Gels with grouped hydrophobic residues performed equally with those of alternating hydrophobicity and E residues in the case of VVEA and VEVA, with measured moduli of 92.7 ± 20.4 kPa (VVEA) and 85.5 ± 8.1 kPa (VEVA) before polymerization. A preference for alternating hydrophobicity appears in the case of V gels with D residues, as VVDA has a lower storage modulus (74.1 ± 4.3 kPa) compared to that of VDVA (117 ± 16.0 kPa) before polymerization. After polymerization, PVEVA possessed a measured modulus 32.1 kPa higher than that of PVVEA (67.9 ± 2.1 kPa versus 35.8 ± 7.7 kPa); only two replicates were measured for PVEVA, but the narrow error margins suggest that the average value is accurate. A 56.9 kPa decrease was observed in the modulus of PVVEA after polymerization (35.8 ± 7.7 versus 92.7 ± 20.4 before polymerization). V-based gels containing D residues exhibited a slight preference for grouped hydrophobic residues, as PVVDA exhibits a 16.9 kPa greater modulus than PVDVA (117 ± 3.9 versus 100.1 ± 6.7 respectively). The effects of hydrophobic residue placement and

acidic residue identity appear to interact in V gels, leaving no clear method to predict which V-based sequence will possess the highest moduli when considering a library.

Overall, V-based sequences were superior to I-based sequences in almost every case before polymerization, with the single exception observed in unpolymerized IEIA exhibiting a higher modulus (97.8 ± 14.5 kPa) than VEVA (85.5 ± 8.1 kPa). V gels consistently demonstrated higher storage moduli than I gels after polymerization, with the greatest disparity observed between PVVDA (117 ± 3.9 kPa) and PIIDA (27.8 ± 5.3 kPa). PVVDA exhibited the highest storage modulus at 117 kPa, followed by VDVA measured at 100 kPa. Apart from IIEA and VVDA, samples showed a decrease in storage modulus after polymerization. Gels were expected to have higher moduli after polymerization due to the extensive network of covalent bonds distributed throughout the gel by the polymer chains, but only two samples showed an increase in modulus post-polymerization. General trends observed in loss moduli followed those described above for storage moduli (Appendix C, CF2). All gels reached a maximum storage modulus at high angular frequency (Figure 9), and all gels were shear thinning (Appendix C, CF3), indicating potential injectability.²⁰

Table 5. Average storage moduli of 1% (w/v) peptide hydrogels

Peptide	Unpolymerized (kPa)	Polymerized (kPa)
VEVA	85.5 ± 8.1	67.9 ± 2.1*
VVEA	92.7 ± 20.4	35.8 ± 7.7
IEIA	97.8 ± 14.5	44.0 ± 14.2
IIEA	20.0 ± 5.7	28.0 ± 8.7
VDVA	116.8 ± 16.0	100.1 ± 6.7
VVDA	74.1 ± 4.3	117.0 ± 3.9
IDIA	94.7 ± 7.8	80.6 ± 19.0
IIDA	35.5 ± 9.0	27.8 ± 5.3

* Two data points

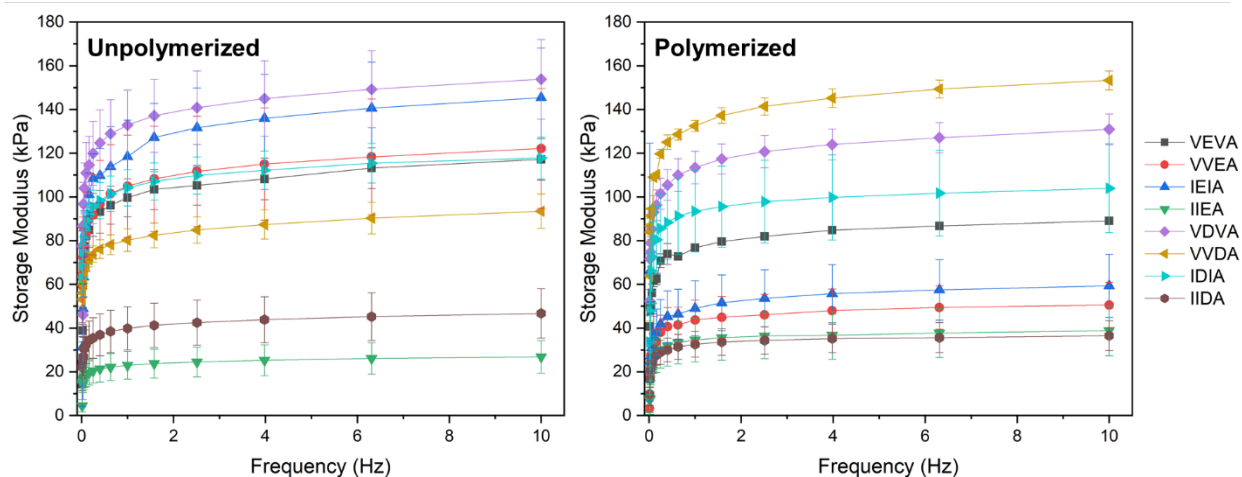


Figure 9. Storage modulus versus angular frequency for unpolymerized and polymerized gels.

Rheological testing indicates that 1% by weight hydrogels made from this peptide library possess biologically relevant moduli after polymerization. The polymerized gels, ranging in moduli from 20-120 kPa, fall in the same range as breast (2-20 kPa), brain (30-100 kPa) and

heart tissues (10-5000 kPa).²¹ Though further testing is required to assess biocompatibility, these results are promising for the development of a conductive hydrogel for tissue engineering applications.

Conclusions

A library of 12 N-acylated thiophene-peptide hybrids was synthesized, eight of which successfully self-assembled into beta-sheet containing gels in the presence of exogenous EDOT-OH. The resulting gels were polymerized with FeCl₃, yielding gels with conductivity approaching that of pure CP and undoped silicon. Gels retained beta-sheet content and a fibrous structure after polymerization, leading to mechanical properties in the range of human soft tissues such as brain and heart. The two unpolymerized gels predicted to possess the highest mechanical properties based on known beta-sheet forming sequences exhibited the highest storage moduli before polymerization. A clear pattern was not observed in storage moduli following polymerization, as most polymerized gels exhibited a decrease in moduli compared to their unpolymerized counterparts. These observations require additional exploration before intentional peptide design becomes feasible.

Future work for this project includes control testing to determine whether a CP moiety must be chemically attached to the peptide in order for the self-assembly process to template the CP. By replacing the thiophene group at the N-termini of the peptides with a benzene group that cannot participate in polymerization, a second library will be synthesized and interrogated for electrical, mechanical, and morphological features. Furthermore, while initial mechanical testing indicates that these hydrogels are shear-thinning, further mechanical testing is necessary to determine whether their viscosity is appropriate for injections delivered in a clinical setting. This testing involves both additional rheological experiments (e.g. strain sweep, cyclic strain sweep) and

injection force measurements when delivered through needles of various gauge. Finally, determining the biocompatibility of these materials is necessary before their introduction as an alternative to traditional metal electrodes.

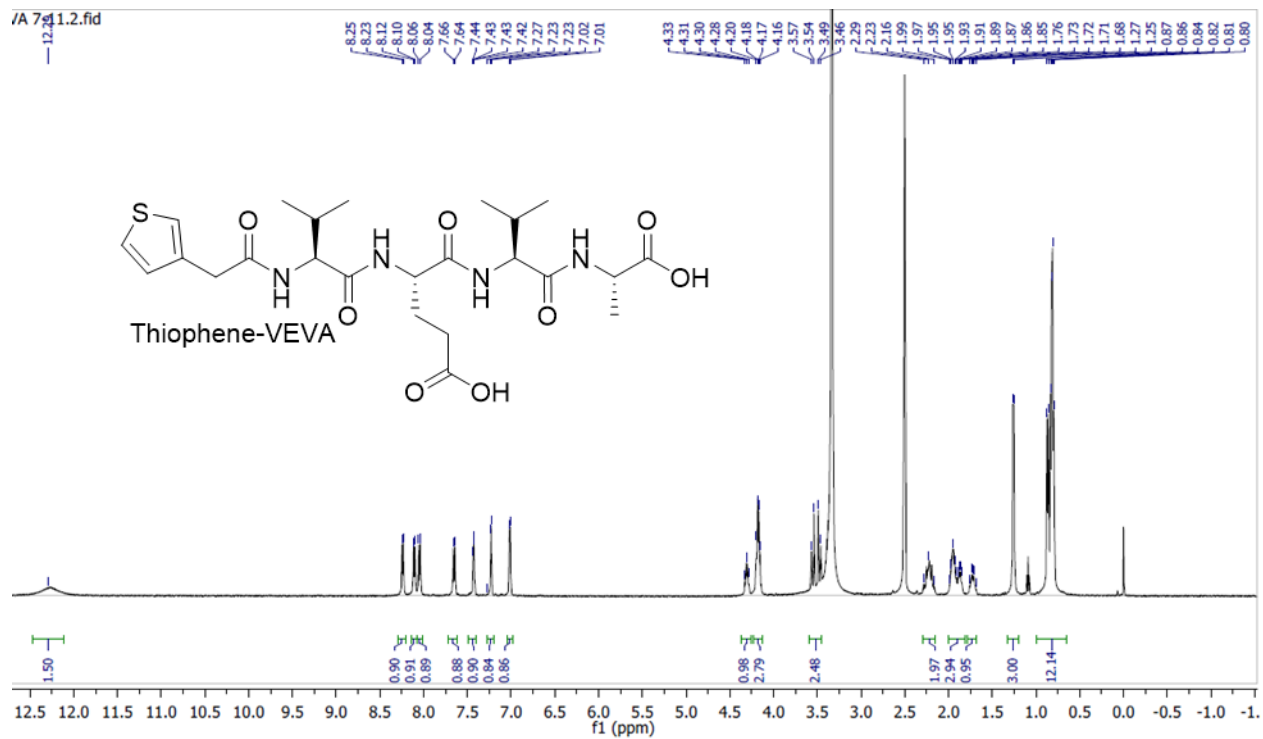
Works Cited

1. Asplund, M.; Nyberg, T.; Inganäs, O. Electroactive polymers for neural interfaces. *Polym. Chem.*, **2010**, *1*, 1374-1391.
2. Ravichandran, R.; Sundarajan, S.; Venugopal, J. R.; Mukherjee, S.; Ramakrishna, S. Applications of Conducting Polymers and Their Issues in Biomedical Engineering. *J. R. Soc., Interface*, **2010**, *7*, S559-S579.
3. Escuder, B.; Miravet, J.F. Silk-Inspired Low-Molecular-Weight Organogelator. *Langmuir*, **2006**, *22*, 7793-7797.
4. Triguero, J.; Zanuy, D.; Aleman, C. Conformational analysis of a modified RGD adhesive sequence. *J. Pept. Sci.*, **2016**, *23*, 172-181.
5. Hamedi, M.; Wigenius, J.; Tai, F-I.; Bjork, P.; Aili, D. Polypeptide-guided assembly of conducting polymer nanocomposites. *Nanoscale*, **2010**, *2*, 2058-2061.
6. Hardy, J. G.; Scheibel, T. R. Silk-inspired polymers and proteins. *Biochem. Soc. Trans.*, **2009**, *37*, 677-681.
7. Schillinger, E-K. (2010): Peptide-and amino acid-directed self-assembly of oligothiophenes. Open Access Repository der Universität Ulm. Dissertation. DOI: 10.18725/OPARU-1860.

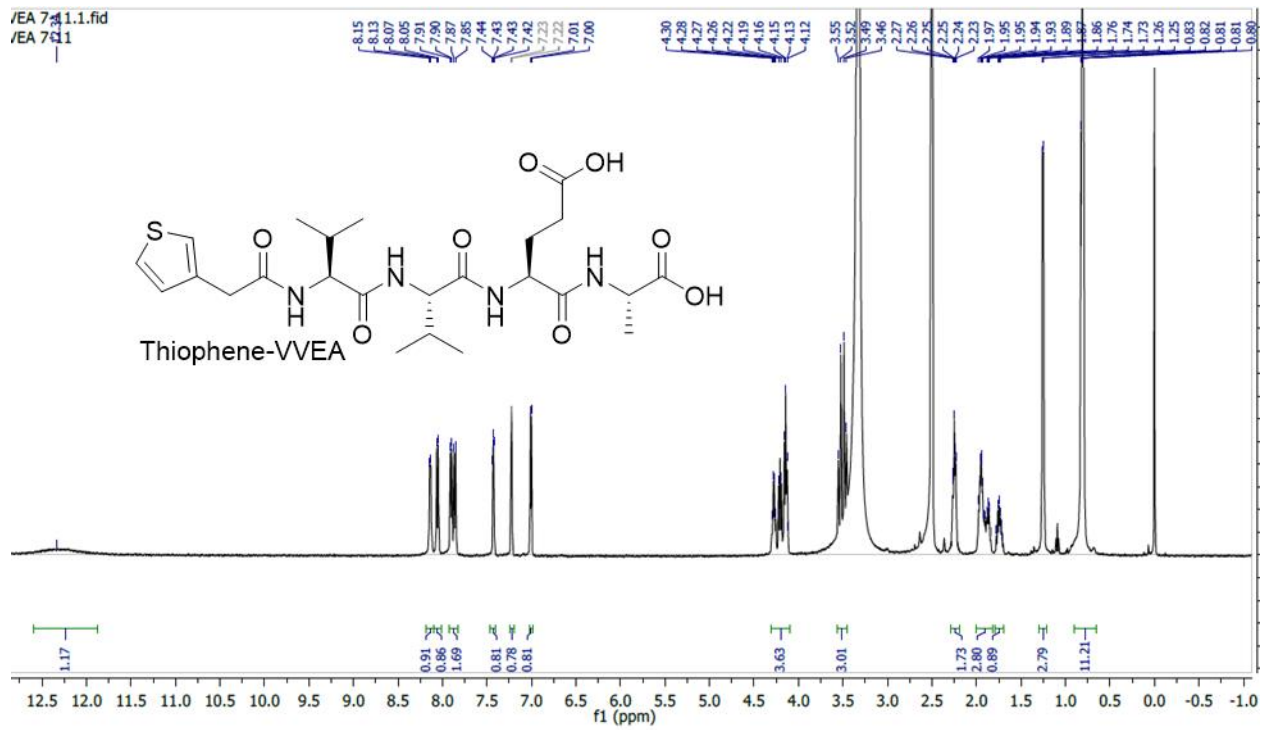
8. Vandermeulen, G. W. M.; Klok, H-A. Peptide/Protein Hybrid Materials: Enhanced Control of Structure and Improved Performance through Conjugation of Biological and Synthetic Polymers. *Macromol. Biosci.*, **2004**, *4*, 383-398.
9. Shaytan, A. K. et al. Self-organizing bioinspired oligothiophene-oligopeptide hybrids. *Beilstein J. Nanotechnol.*, **2011**, *2*, 525-544.
10. Blatz, T. J.; Fry, M. M.; James, E. I.; Albin, T. J.; Pollard, Z.; Kowalczyk, T.; Murphy, A. R. Templating the 3D structure of conducting polymers with self-assembling peptides. *J. Mater. Chem. B*, **2017**, *5*, 4690-4696.
11. Mandal, D.; Shirazi, A. N.; Parang, K. Self-Assembly of Peptides to Nanostructures. *Org. Biomol. Chem.*, **2014**, *12*, 3544-3561.
12. Klok, H.A.; Rosler, A.; Gotz, G.; Mena-Osteritz, E.; Bauerle, P. Synthesis of a silk-inspired peptide oligothiophene conjugate. *Org. Biomol. Chem.*, **2004**, *2* (24), 3541-3544.
13. Gus'kova, O.A.; Khalatur, P.G.; Bauerle, P.; Khokhlov, A.R. Silk-inspired 'molecular chimeras': Atomistic simulation of nanoarchitectures based on thiophene-peptide copolymers. *Chem. Phys. Lett.*, **2008**, *461* (1-3), 64-70.
14. Ekiz, M. S.; Cinar, G.; Khalily, M. A.; Guler, M. O. Self-assembled peptide nanostructures for functional materials. *Nanotechnology*. **2016**, *27*, 402002-402039.
15. Hu, X.; Kaplan, D.; Cebe, P. Determining Beta-Sheet Crystallinity in Fibrous Proteins by Thermal Analysis and Infrared Spectroscopy. *Macromolecules*. **2006**, *39*, 6161-6170.
16. Pal, R. K.; Turner, E. E.; Chalfant, B. H.; Yadavalli, V. K. Mechanically robust, photopatternable conductive hydrogel composites. *React. Funct. Polym.*, **2017**, *120*, 66-73.

17. Han, L.; Liu, K.; Wang, M.; Wang, K.; Fang, L.; Chen, H.; Zhou, J.; Lu, X. Mussel-inspired adhesive and conductive hydrogel with long-lasting moisture and extreme temperature tolerance. *Adv. Funct. Mater.*, **2018**, *28*, 1704195
18. Aulisa, L.; Dong, H.; Hartgerink, J. D. Self-assembly of multidomain peptides: sequence variation allows control over cross-linking and viscoelasticity. *Biomacromolecules*, **2009**, *10*, 2694-2698.
19. Jung, J. P.; Nagaraj, A. K.; Fox, E. K.; Rudra, J. S.; Devgun, J. M.; Collier, J. H. Co-assembling peptides as defined matrices for endothelial cells. *Biomaterials*, **2009**, *30*(12) 1-11.
20. Chen, M. H.; Wang, L. L.; Chung, J. J.; Kim, Y.; Atluri, P.; Burdick, J. A. Methods to Assess Shear-Thinning Hydrogels for Application As Injectable Biomaterials. *ACS Biomater. Sci. Eng.* **2017**, *3*(12), 3146-3160.
21. Kim, H. N.; Kim, M. S.; Jiao, A.; Kim, D. H.; Suh, K. Y. Patterning methods for polymers in cell and tissue engineering. *Ann. Biomed. Eng.*, **2012**, *40*, 1339-1355.
22. Tena-Solsona, M.; Miravet, J. F.; Escuder, B. Tetrapeptidic Molecular Hydrogels: Self-assembly and coaggregation with Amyloid Fragment A β 1-40. *Chem.-Eur. J.*, **2014**, *20* (4), 1023-1031.

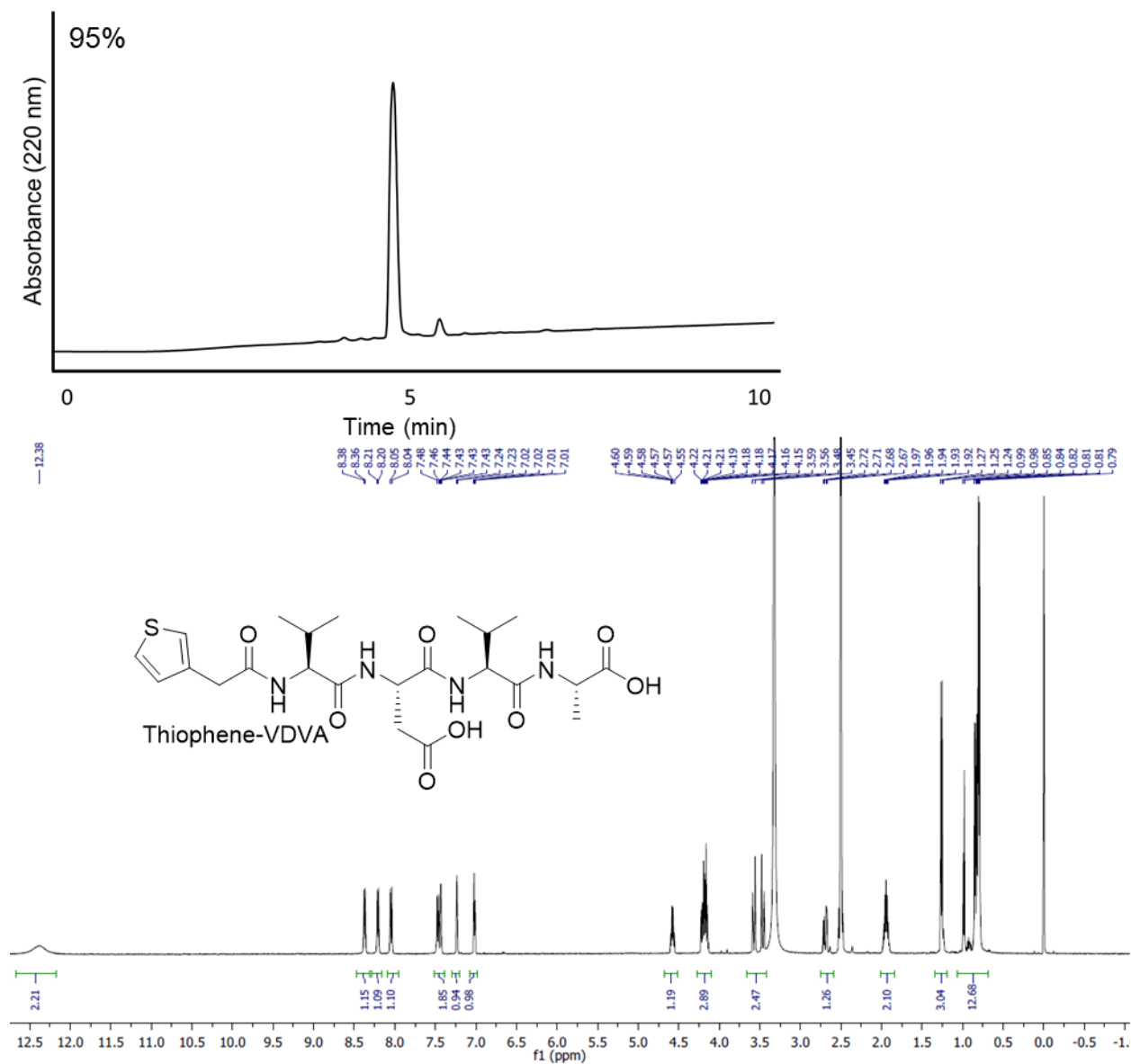
Appendix A



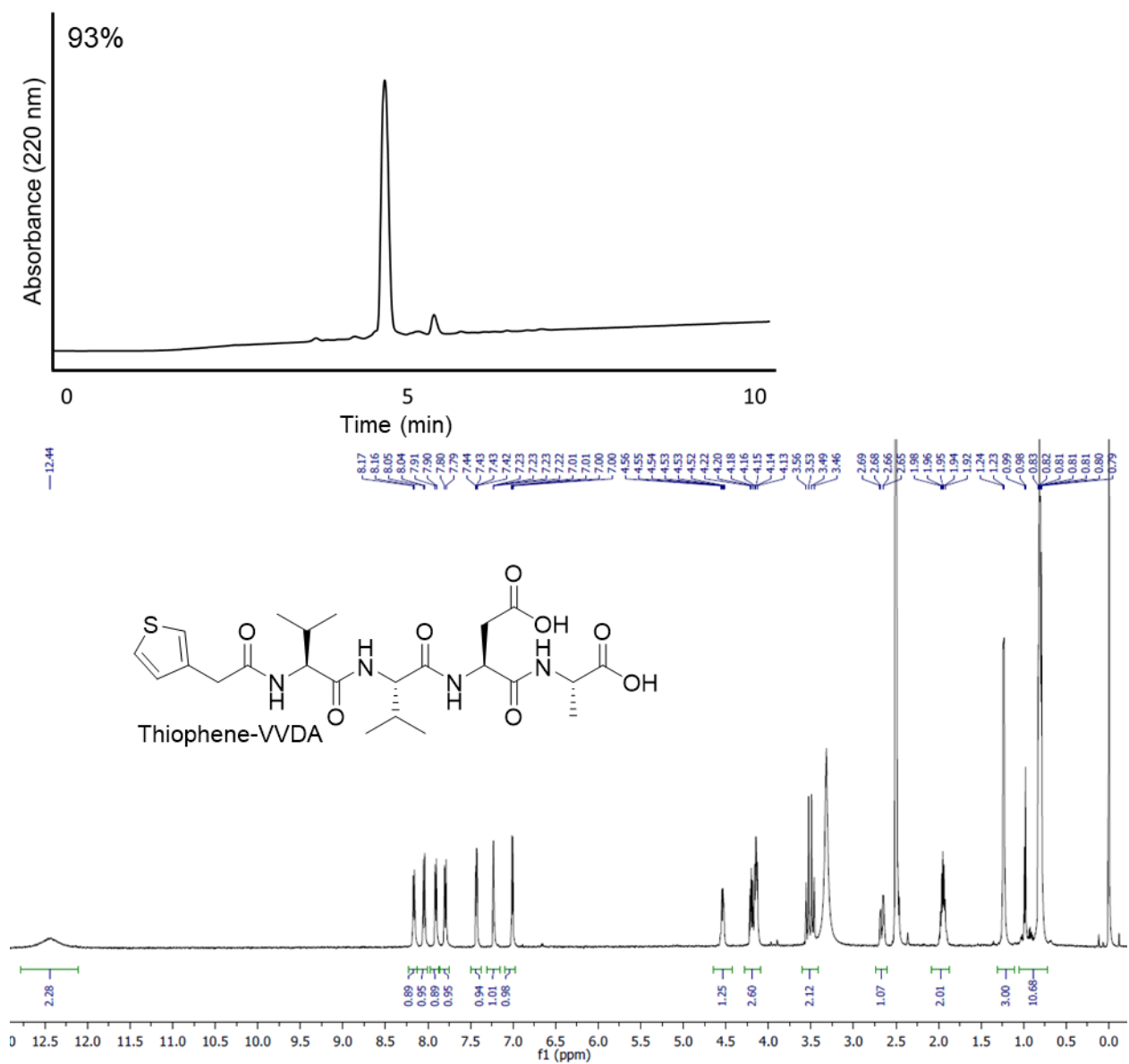
AF1. ¹H NMR spectrum of thiophene-VEVA.



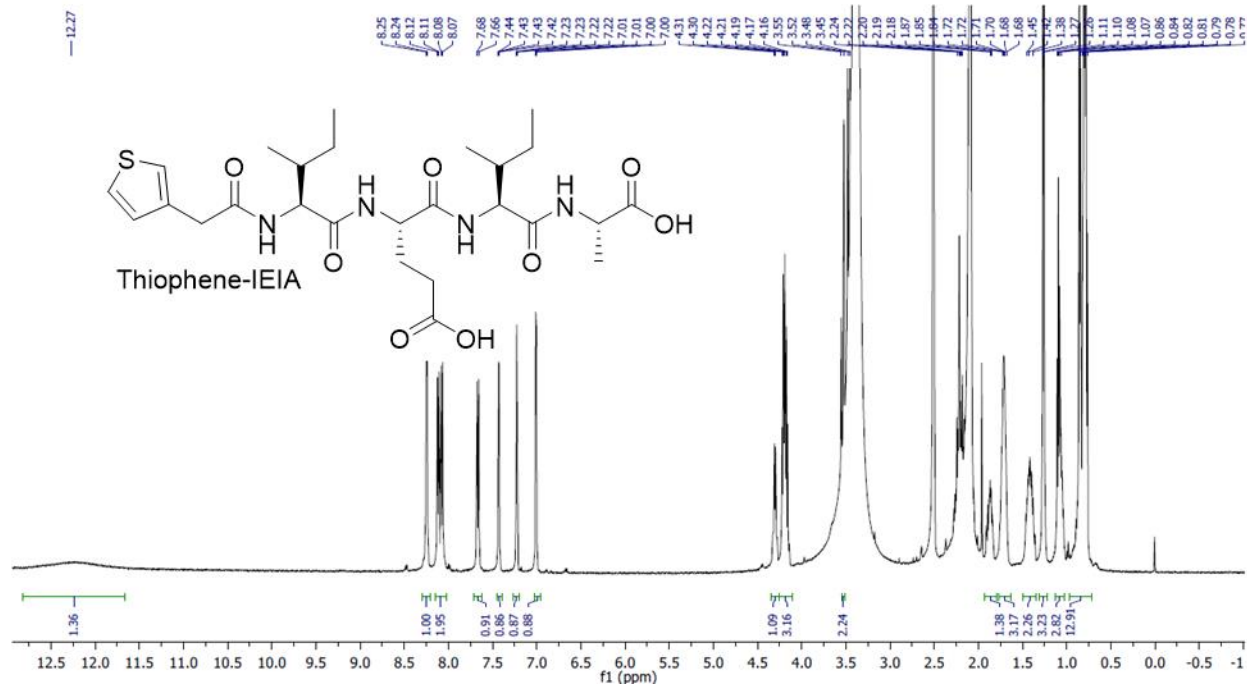
AF2. ¹H NMR spectrum of thiophene-VVEA.



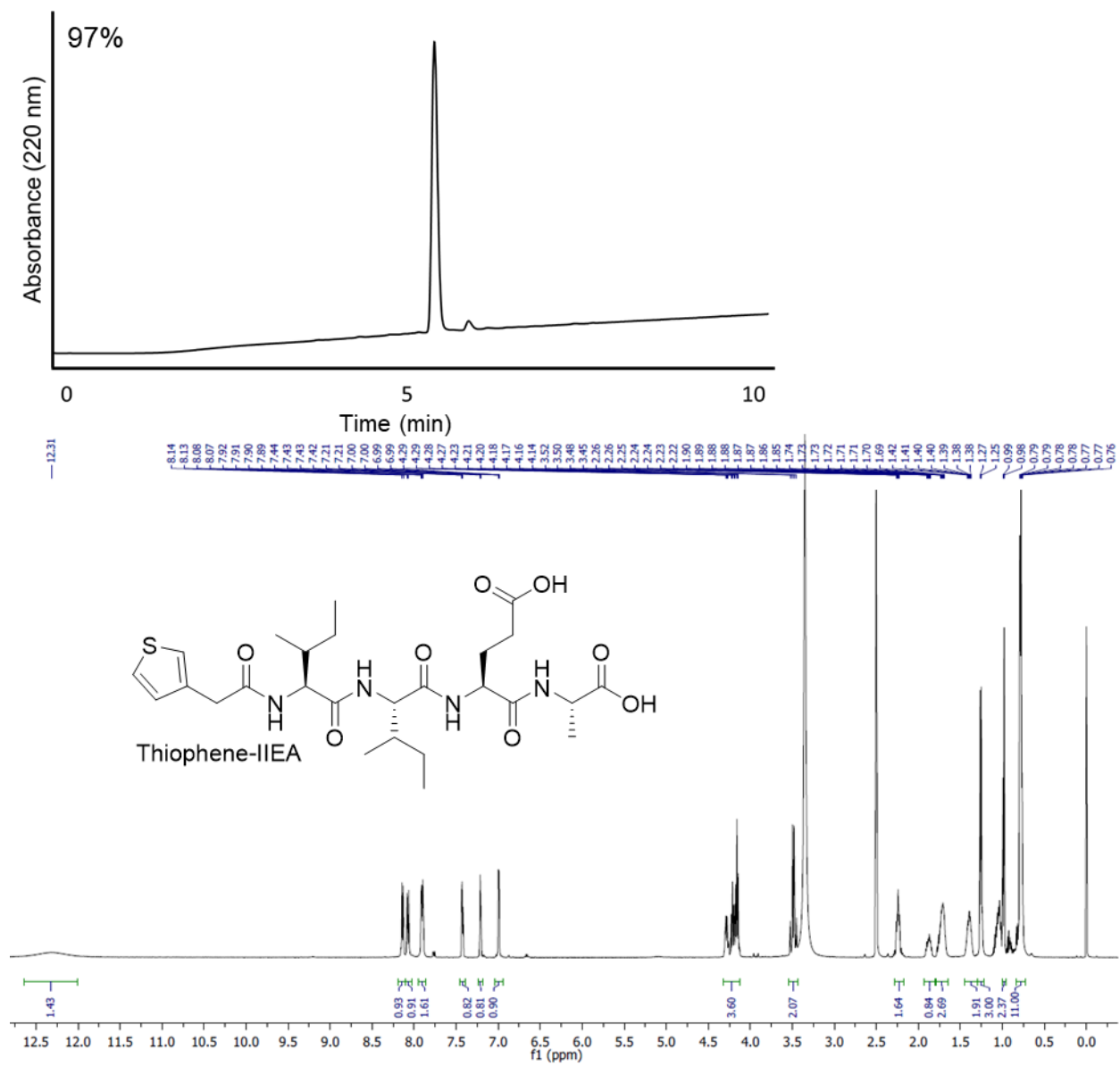
AF3. RP-HPLC trace of thiophene-VDVA showing 95% purity (top). ¹H NMR spectrum of thiophene-VDVA (bottom).



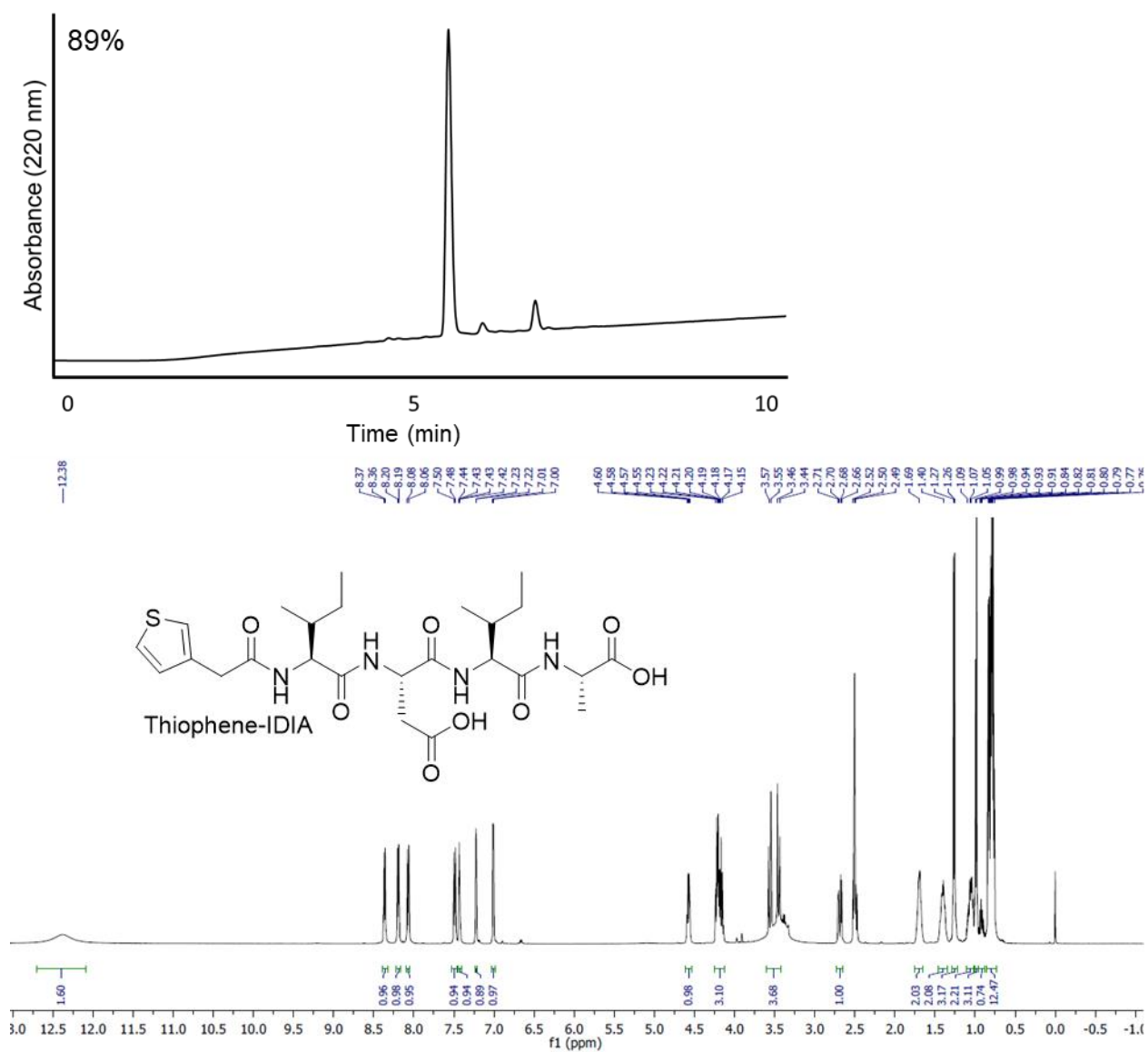
AF4. RP-HPLC trace of thiophene-VVDA showing 93% purity (top). ¹H NMR spectrum of thiophene-VVDA (bottom).



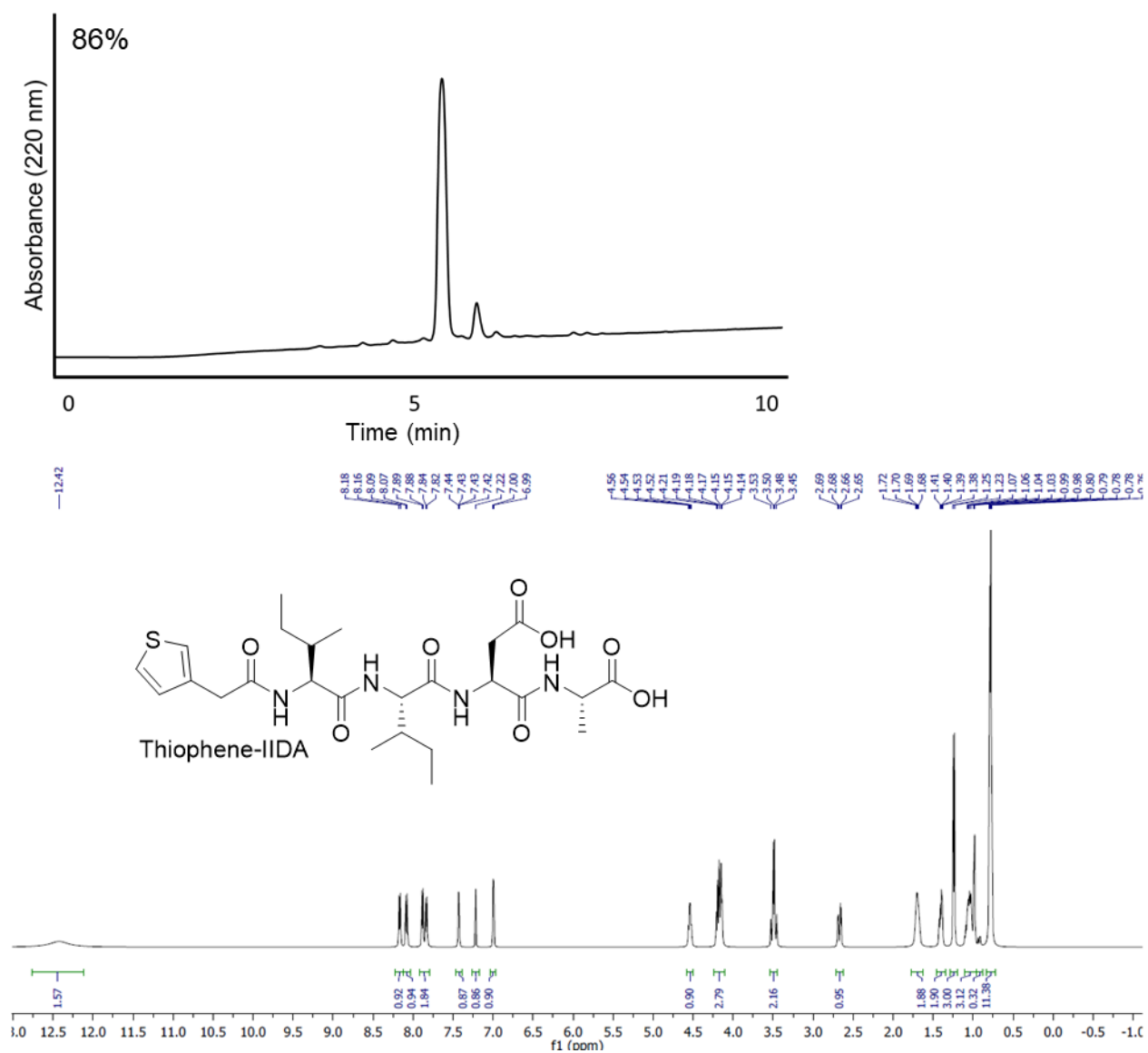
AF5. ^1H NMR spectrum of thiophene-IEIA.



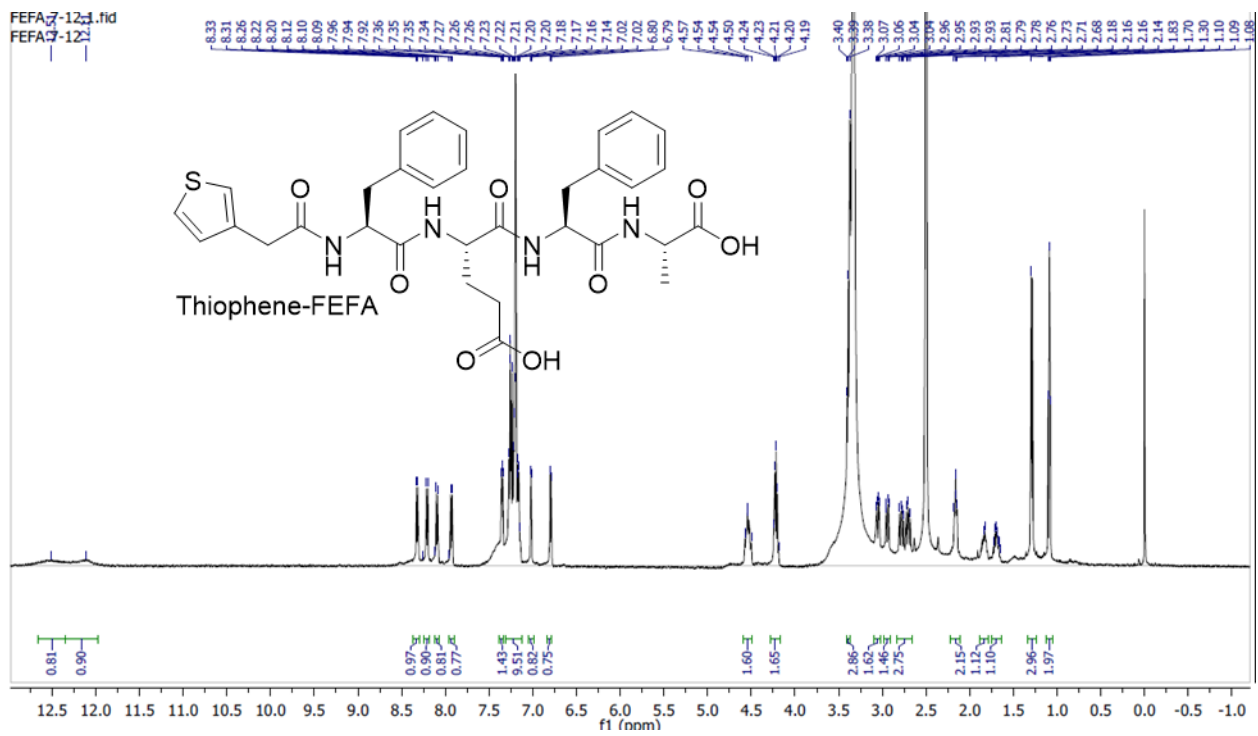
AF6. RP-HPLC trace of thiophene-IIIEA showing 97% purity (top). ¹H NMR spectrum of thiophene-IIIEA (bottom).



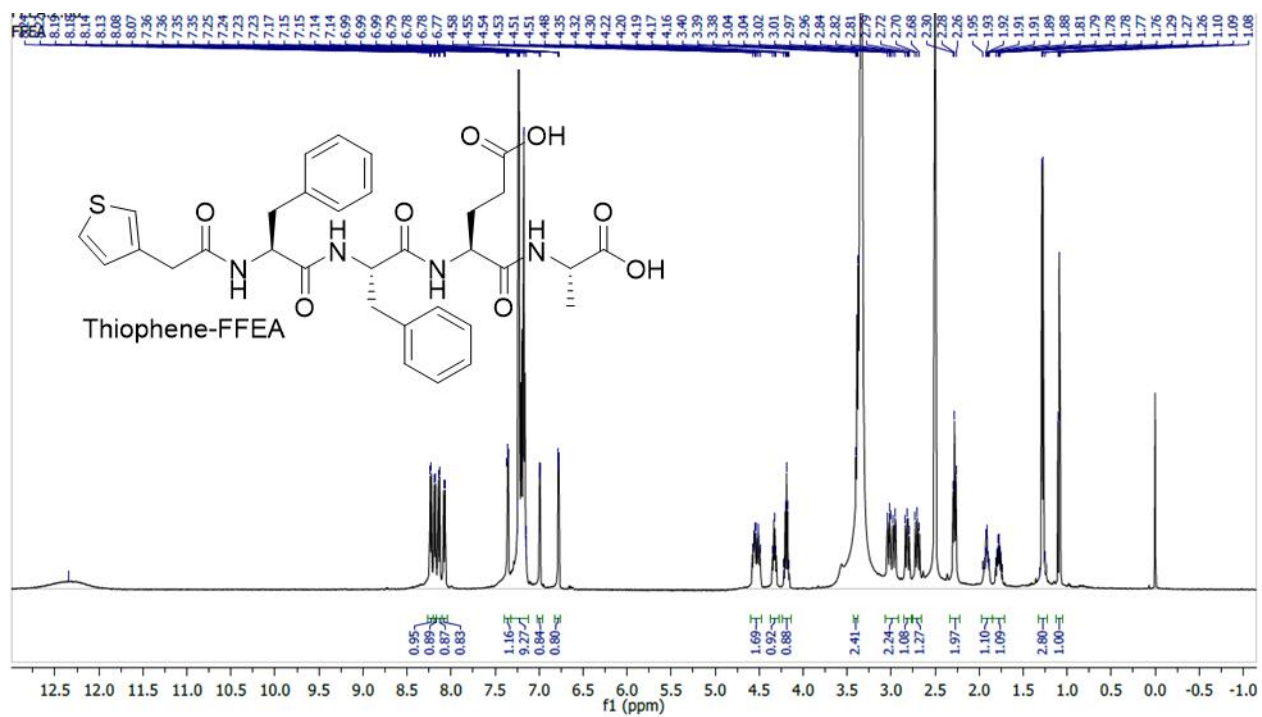
AF7. RP-HPLC trace of thiophene-IDIA showing 89% purity (top). ¹H NMR spectrum of thiophene-IDIA (bottom).



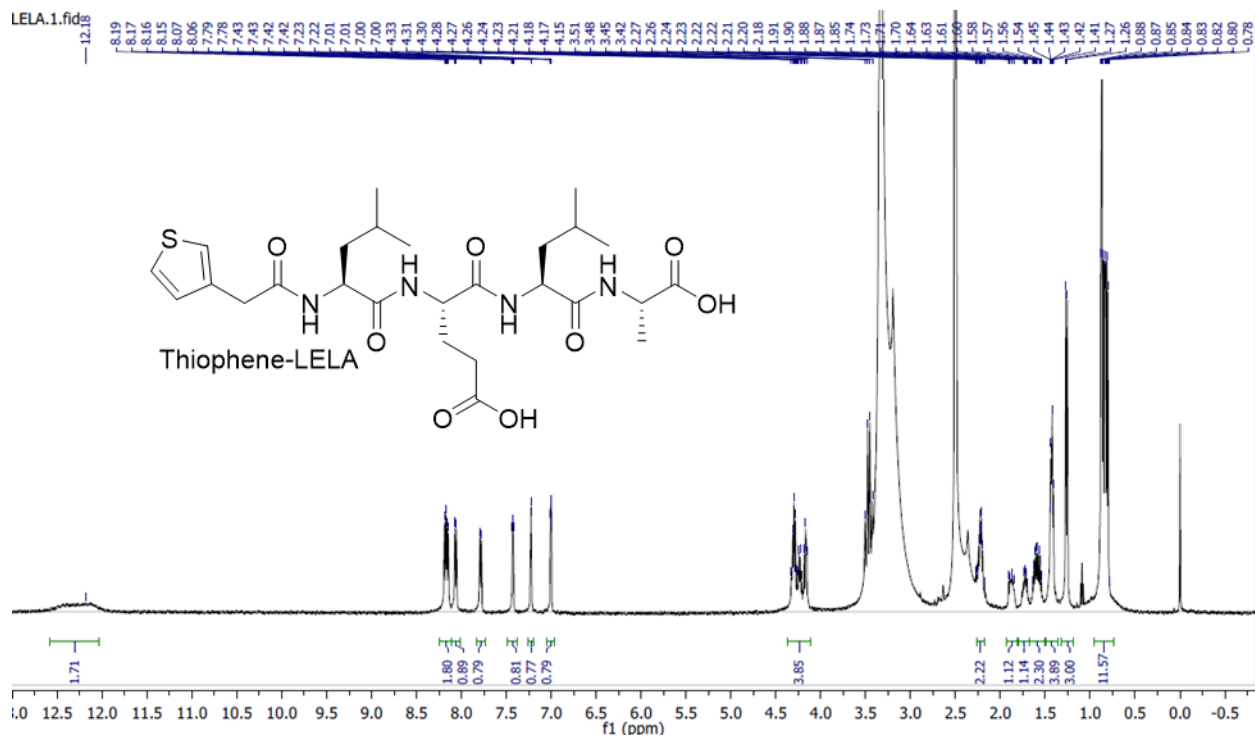
AF8. RP-HPLC trace of thiophene-IIDA showing 86% purity (top). ¹H NMR spectrum of thiophene-IIDA (bottom).



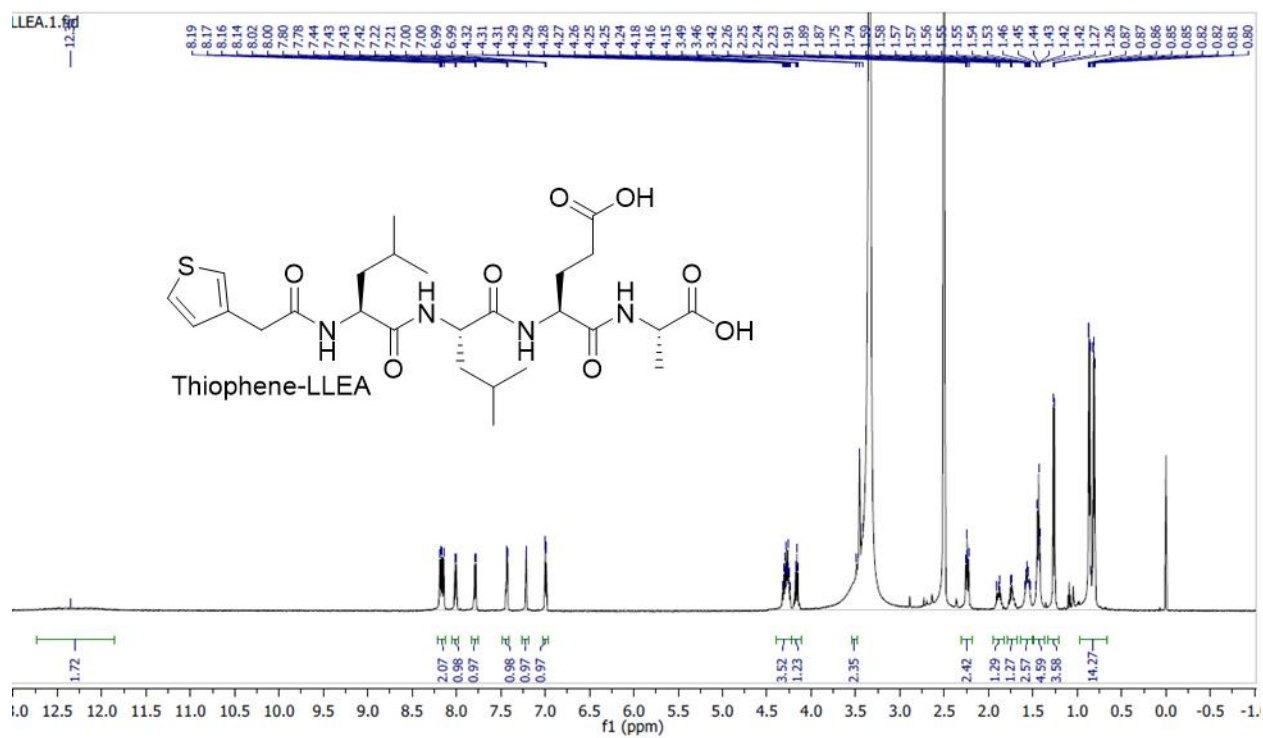
AF9. ^1H NMR spectrum of thiophene-FEFA.



AF10. ^1H NMR spectrum of thiophene-FFEA.



AF11. ¹H NMR spectrum of thiophene-LELA.



AF12. ¹H NMR spectrum of thiophene-LLEA.

Appendix B

FEFA and FFEA Gelation Attempts

FEFA and FFEA (Fig. 1) were gelled at four different concentrations (0.75%, 1%, 1.5%, and 3% (w/v)) following standard procedure and utilizing the components listed in Table BT1. No homogenous gels were observed, and peptide began to precipitate from the gels over the course of 30 min to several hours. The 3% gels remained intact for the longest amount of time, but still completely collapsed after seven hours undisturbed. It is hypothesized that initial assembly corresponds to the sorting of the hydrophobic and hydrophilic residues into beta-sheets, while the disruption in structure arises from pi-stacking between the aromatic phenyl rings. Heating the peptide solution during gelation did not prolong the stability of the gels and gels could not be reformed by sonicating and heating the collapsed solution.

LELA and LLEA Gelation Attempts

Likewise, thiophene-LELA gelation was attempted at 0.44% and 1.5 % (w/v) (BT1), but no gelation was observed in any case. Acidification resulted in immediate precipitation. Mixing thiophene-LELA at 0.7% (w/v) with 1:1 EDOT-OH and utilizing the buffered acid addition necessary to gel the phenylalanine peptide isomers did not result in the immediate formation of a gel (BT2). The aqueous solutions were left to rest overnight, which did not result in gelation. A subsequent addition of 100 μ L *p*-TSA (0.2 M) resulted in precipitation. Thiophene-LELA and -LLEA did not form stable gels under any conditions.

BT1. Phenylalanine and leucine gel study

Peptide	Peptide Mass (mg)	[Gel] (w/v)	np H ₂ O (μL)	1 M NaOH (μL)	0.2 M <i>p</i> -TSA (μL)	Homogenous Gel?
FEFA	3.8	0.75%	365	15.0	120	No
FFEA	3.8	0.75%	365	15.0	120	No
FEFA	5.0	1.00%	80.0	5.0	415	No
FFEA	5.0	1.00%	250	30.0	220	No
FEFA	7.5	1.50%	250	30.0	220	No
FFEA	7.5	1.50 %	250	30.0	220	No
FEFA	15	3.00%	260	49.0	193†	No
FFEA	15	3.00%	260	49.0	193†	No
LELA	2.5	0.44%	80.0	5.0	415	No
LLEA	5.0	1.00%	250	30.0	220	No

† 0.5 M *p*-TSA

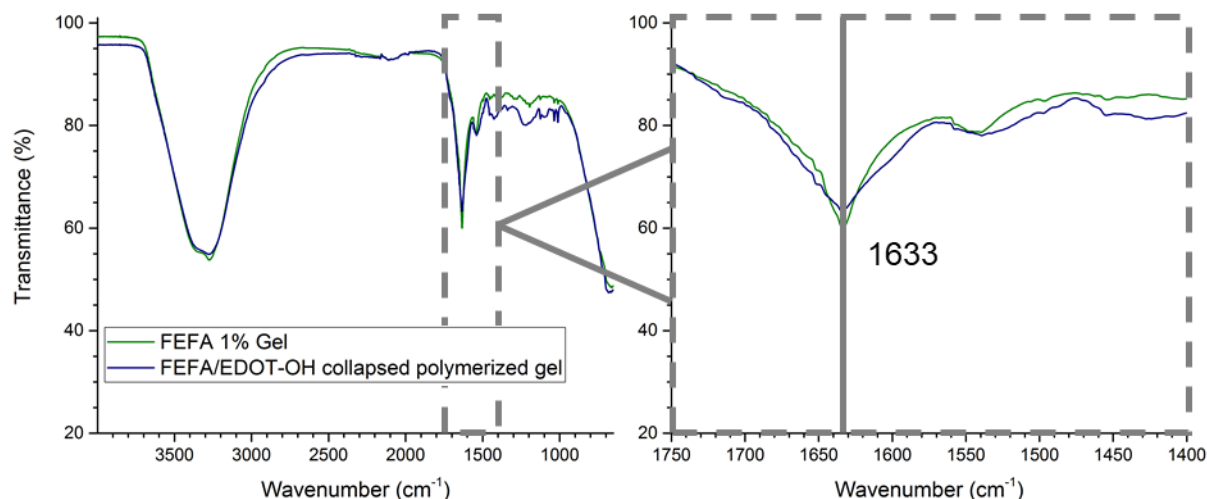
A literature search concerning peptides with similar primary sequences to the peptide isomers in question indicated robust assembly achieved by lowering the solution pH very slowly, or hydrolyzing a lactone to evenly distribute protons throughout the aqueous peptide solution.²² To test that method, FEFA was dissolved in a sodium carbonate buffer solution, to which *p*-TSA (0.2 M) was added via a micropipette over several hours to induce gelation (BT2). Thiophene-FEFA gelled strongly at 1.5% (w/v) using this method, prompting attempts to use the same method to form phenylalanine gels with 1:1 EDOT-OH. These experiments resulted in a transient gel that precipitated and collapsed before polymerization was complete. The FTIR spectra of the intact gel and the collapsed polymerized gel are nearly identical, both showing amide I peaks at 1633 cm⁻¹ (BF1). This peak is indicative of beta-sheet content, but the collapsed

gel indicates that the hydrogen bonds between the beta-sheets were not enough to result in a robust, stable gel.

Buffered Gelation Procedure: Lyophilized peptide-thiophene derivatives and sodium carbonate (1:2 mol ratio) were dissolved in npH₂O while sonicating. Two molar equivalents of 0.2 M *p*-TSA were added via a micropipette (5 μL/15 min) while sonicating and maintaining the bath temperature at 20 °C. Additional acid was added in one aliquot to induce gelation (BT2).

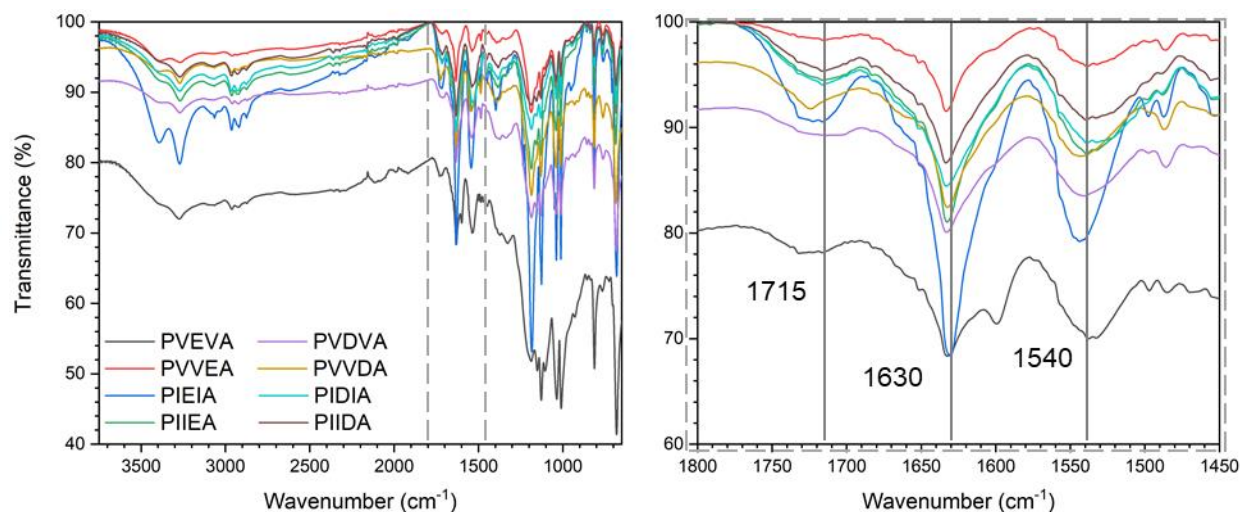
BT2. Buffered gel components

Peptide	Peptide Mass (mg)	EDOT-OH Mass (mg)	NaHCO ₃ Mass (mg)	[Gel] (w/v)	np H ₂ O (μL)	0.2 M <i>p</i> -TSA (μL)	Homogenous Gel?
LELA	3.5	1.1	1.4	0.70%	440	60.0	No
LLEA	5.0	1.5	1.9	1.00%	355	145	No
FEFA	7.5	2.1	2.5	1.50%	265	235	Transient



BF1. FTIR spectra of wet thiophene-FEFA gels showing retention of beta-sheet assembly before and after polymerization and collapse.

Appendix C



CF1. FTIR spectra of polymerized gels indicating retention of beta-sheet assembly.

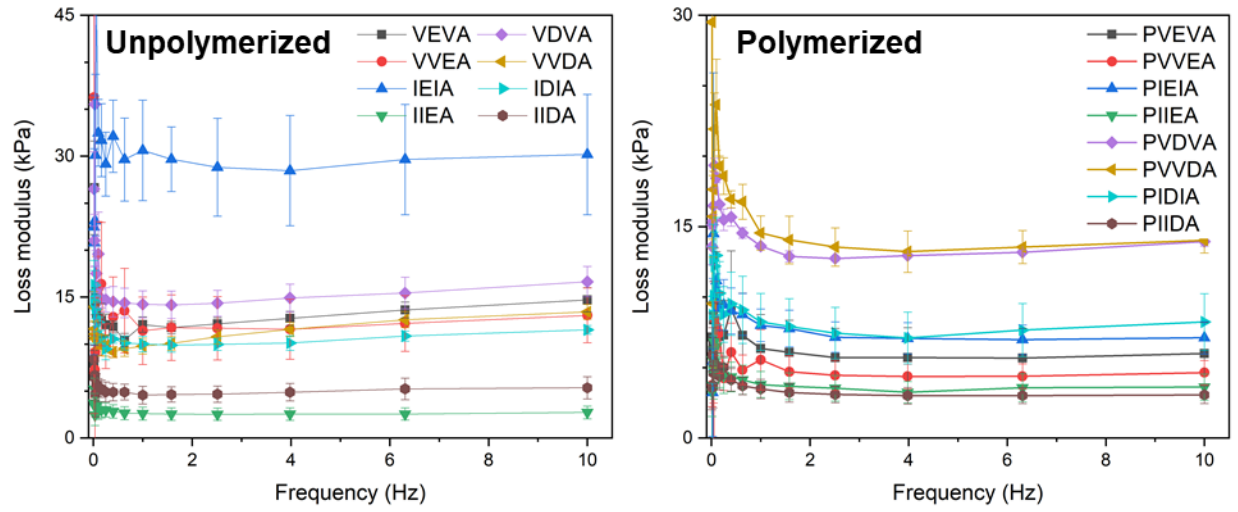
Equation 1. $\rho = s * d$

Where ρ is resistivity, s is the average measured sheet resistivity, and d is pellet thickness in cm.

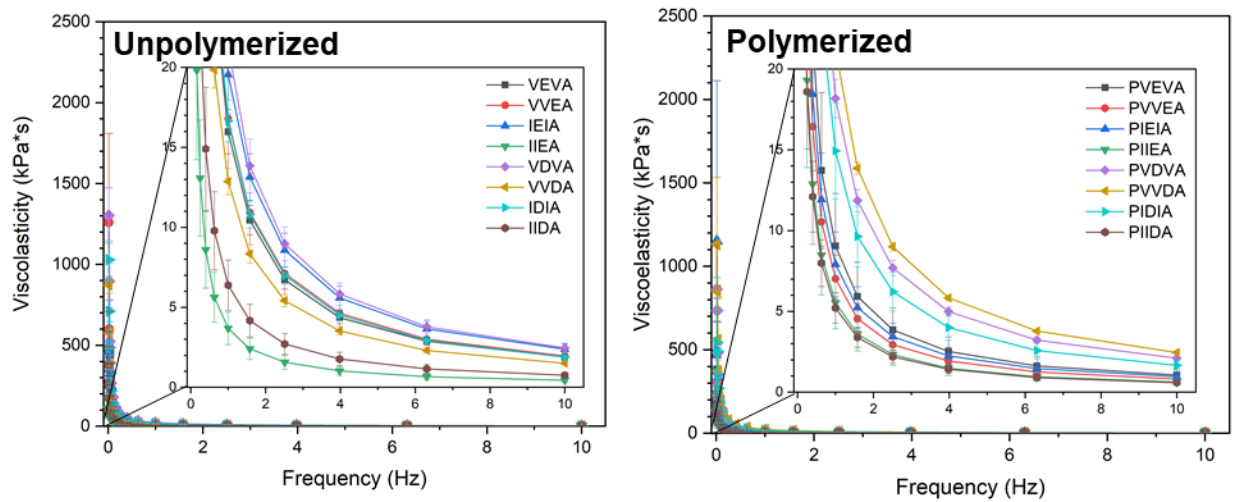
Equation 2. $\sigma = \rho^{-1}$

Where σ is conductivity and ρ is resistivity.

The loss modulus of a gel relates to its ability to dissipate energy through stress relaxation.²⁰ PVDVA and PVVDA exhibited the highest loss moduli at approximately 15 kPa (CF2), followed by PIDIA and PIEIA at approximately 8 kPa. This pattern is also observed in the viscoelasticity of samples following polymerization (CF3), a parameter that gives insight into injectability of the tested hydrogels. All gels were shear-thinning, indicating potential injectability, but the magnitude of force required to extrude the gels from a syringe remains to be tested before assessing clinical relevance. A balance between storage modulus, loss modulus, and viscoelasticity must be achieved for successful injection.²⁰



CF2. Loss moduli of gels pre- and post-polymerization indicating a similar trend in assembly strength as observed in storage moduli.



CF3. Viscoelasticity of gels pre-and post-polymerization highlighting the shear-thinning properties of the library necessary for injectability.